

Impurity Effects on Superconductivity on Surfaces of Topological Insulators

Yuto ITO, Youhei YAMAJI, and Masatoshi IMADA

Department of Applied Physics, University of Tokyo, Bunkyo, Tokyo 113-8656, Japan

A two-dimensional superconductor (SC) on surfaces of topological insulators (TIs) is a mixture of s -wave and helical p -wave components when induced by s -wave interactions, since spin and momentum are correlated. On the basis of the Abrikosov-Gor'kov theory, we reveal that unconventional SCs on the surfaces of TIs are stable against time-reversal symmetric (TRS) impurities within a region of small impurity concentration. Moreover, we analyze the stability of the SC on the surfaces of TIs against impurities beyond the perturbation theory by solving the real-space Bogoliubov-de Gennes equation for an effective tight-binding model of a TI. We find that the SC is stable against strong TRS impurities. The behaviors of bound states around an impurity suggest that the SC on the surfaces of TIs is not a topological SC.

KEYWORDS: topological insulator, helical Dirac electron, unconventional superconductivity, impurity scattering, time reversal symmetry, spin orbit interaction, Abrikosov-Gor'kov theory, Bogoliubov-de Gennes equation, impurity induced state

1. Introduction

Three-dimensional (3D) topological insulators (TIs) have two-dimensional (2D) surface states (SSs) topologically protected by the time reversal symmetry (TRS).^{1,2} The existence of SSs is characterized by Z_2 topological invariants, which are determined by the band structure of the bulk.³⁻⁶ In most cases, strong spin orbit interactions (SOIs) play important roles in constructing topologically nontrivial band structures and induce TIs. By SOIs, helical spin structures in momentum space are observed, i.e., helical Dirac electrons are generated. Helical Dirac electrons in TIs have been verified through observations of energy dispersions of Dirac SSs by angle-resolved photoemission spectroscopy (ARPES).⁷⁻¹⁰

Superconductivity on the surfaces of TIs attracts attention as one type of 2D unconventional superconductivity. An unconventional superconductor (SC) is a mixture of s -wave and helical p -wave components, since in helical Dirac electron systems, spin and momentum are correlated.¹¹ Such a SC is possibly induced by a proximity effect from an s -wave SC to a TI^{12,13} or, in other words, by an s -wave attractive interaction,¹¹ when the Fermi energy is away from the Dirac point. This SC formally resembles a spinless chiral p -wave SC that breaks TRS¹⁴ in the representation where the Dirac electron dispersion is diagonalized. The difference is that the SC on the surfaces of TIs does not break TRS. From that similarity of the two SCs, an unconventional SC on the SSs of TI is proposed for application to quantum computations using Majorana bound states caused by the proximity effect between a superconductor and the surface states of TI.¹² Introducing superconductivity into the surfaces of TIs has been a challenge in experimental research. For example, toward this goal, a SC has been realized in Cu-doped Bi₂Se₃,^{15,16} although the existence of a surface SC is not confirmed yet. Recently, it has been reported that superconductivity is introduced into Bi₂Se₃ thin films by the superconductivity proximity effect.¹⁷

In realizing such a SC, the stability of the SC is an

important problem. In particular, impurity effects are relevant to the stability since surfaces on TI frequently contain disorders such as defects or impurity potentials. Moreover, on surfaces of TIs, there are facets or steps with disordered boundaries. For example, by scanning tunneling spectroscopy (STS) studies of the surfaces of Bi₂Te₃, one of TIs, an abrupt change in the local density of states (LDOS) was observed near a step structure.¹⁸

Moreover, studies of the stability against impurities allow us to clarify the fundamental physics of a SC on the surfaces of TIs since the stability of the SC depends on the symmetries of the order parameter and on impurities. For example, conventional s -wave SCs are robust to TRS impurities because pair breaking does not exist if the impurity concentration is small.¹⁹ In contrast, unconventional anisotropic SCs are fragile against TRS impurities because of anisotropic quasiparticle scattering that induces pair breaking.²⁰⁻²³ Such pair breaking is also induced even in s -wave SCs when impurities break TRS.²⁴ For the present SC, the order parameter is a mixture of s -wave and helical p -wave components. We study quasiparticle scattering in an unconventional SC in order to reveal its similarity to or difference from those of other SCs.

The organization of this paper is as follows: In §2, in order to study the fundamental stability of the SC on the surfaces of TIs, we analyze the impurity concentration dependence of the mean-field order parameter in the small concentration range in an idealistic helical Dirac electron model using a perturbation theory referred to as the Abrikosov-Gor'kov (AG) theory.²⁴ We find that such a SC, as well as conventional s -wave SCs, is robust in that the mean-field critical temperature T_c and the mean-field order parameter Δ_0 do not linearly decrease with the TRS impurity concentration.²⁵

In §3, we investigate impurity effects nonperturbatively by solving the real-space Bogoliubov-de Gennes (BdG) equation for the tight-binding model of Bi₂Se₃, which is an effective model of TI.^{26,27} We study the scat-

tering strength and impurity concentration dependences of the SC. Moreover, we show that induced bound states around impurities are not Andreev bound states, which implies that the present SC is not a topological SC. We summarize our study in §4 with a discussion.

2. Perturbative Approach

In order to study impurity effects on the surfaces of TIs using the AG theory, we introduce a 2D helical Dirac electron dispersion as an effective model of SSs with an s -wave attractive interaction and on-site TRS scattering following a previous letter.²⁵ We introduce the s -wave attractive interaction because such an interaction is the most well-known origin of superconductivity, for example, an electron-phonon interaction. Moreover, on-site TRS scattering is introduced because it is one of the simplest impurity scatterings and is useful to study fundamental impurity effects. Thus, our Hamiltonian consists of three parts, i.e., a 2D helical Dirac electron dispersion, \mathcal{H}_0 , an s -wave attractive interaction term, \mathcal{H}_{int} , and an on-site TRS impurity scattering term, \mathcal{H}_{imp} :

$$\mathcal{H} = \mathcal{H}_0 + \mathcal{H}_{\text{int}} + \mathcal{H}_{\text{imp}}. \quad (2.1)$$

In this section, we assume that the 2D helical Dirac electron dispersion is represented as

$$\mathcal{H}_0 = \sum_{\mathbf{k}} c^\dagger(\mathbf{k}) [v_F(\sigma_x k_x + \sigma_y k_y) - \mu I] c(\mathbf{k}), \quad (2.2)$$

with the Fermi velocity $v_F > 0$. We set the Fermi energy $\mu > 0$ in order to consider the branch of Dirac electrons above the Dirac point (called the “+” branch hereafter) and neglect mixture of the two branches. Here, the Pauli matrix $\boldsymbol{\sigma}$ describes the electron spin and $c(\mathbf{k}) = (c_{\mathbf{k}\uparrow} \ c_{\mathbf{k}\downarrow})^T$.

We introduce the representation in the helicity basis (helicity representation) to diagonalize \mathcal{H}_0 . By using the unitary transformation $d_{\mathbf{k},\tau}^\dagger = (c_{\mathbf{k}\uparrow}^\dagger + \tau \exp(i\theta_{\mathbf{k}}) c_{\mathbf{k}\downarrow}^\dagger) / \sqrt{2}$ ($\tau = +$ or $-$), \mathcal{H}_0 is diagonalized as

$$\mathcal{H}_0 = \sum_{\mathbf{k}} d^\dagger(\mathbf{k}) (v_F |\mathbf{k}| \tau_z - \mu) d(\mathbf{k}), \quad (2.3)$$

where τ_z is the z component of the Pauli matrix describing branches of Dirac electrons, $\theta_{\mathbf{k}} = \arg(k_x + ik_y)$, and $d(\mathbf{k}) = (d_{\mathbf{k}+} \ d_{\mathbf{k}-})^T$. The index τ ($\tau = \pm$) represents branches of Dirac electrons. Then, we define the energy $\xi_{\mathbf{k}}$ as the energy of the “+” branch measured from the Fermi energy as $\xi_{\mathbf{k}} = v_F |\mathbf{k}| - \mu$. We neglect the “-” branch and write $d_{\mathbf{k}\pm}^{(\dagger)}$ as $d^{(\dagger)}$ below.

Note that the argument in this section is also applicable to the 2D helical Dirac electron dispersions with different spin-momentum relations. For example, in the SSs of Bi₂Se₃, one of TIs, $\sigma_x k_y - \sigma_y k_x$ is substituted for $\sigma_x k_x + \sigma_y k_y$ in eq. (2.2).^{26,27} In such a case, we have to redefine $\theta_{\mathbf{k}}$ as $\theta_{\mathbf{k}} = \arg(k_x + ik_y) + \frac{\pi}{2}$.

We assume that the s -wave attractive interaction H_{int} is written as

$$\mathcal{H}_{\text{int}} = \frac{1}{2S} \sum_{\mathbf{k}, \mathbf{k}', s, s'} V_{\text{int}}(\mathbf{k}, \mathbf{k}'; s, s') c_{-\mathbf{k}s}^\dagger c_{\mathbf{k}s}^\dagger c_{\mathbf{k}'s'} c_{-\mathbf{k}'s'} \quad (2.4)$$

where S is the size of the 2D system. In this equation,

we assume that

$$V_{\text{int}}(\mathbf{k}, \mathbf{k}'; \downarrow, \uparrow) = V_{\text{int}}(\mathbf{k}, \mathbf{k}'; \uparrow, \downarrow) = \begin{cases} -g & (\xi_{\mathbf{k}}, \xi_{\mathbf{k}'} \in [-\omega_c, \omega_c]) \\ 0 & (\xi_{\mathbf{k}}, \xi_{\mathbf{k}'} \notin [-\omega_c, \omega_c]) \end{cases}, \quad (2.5)$$

$$V_{\text{int}}(\mathbf{k}, \mathbf{k}'; \uparrow, \uparrow) = V_{\text{int}}(\mathbf{k}, \mathbf{k}'; \downarrow, \downarrow) = \begin{cases} -g' & (\xi_{\mathbf{k}}, \xi_{\mathbf{k}'} \in [-\omega_c, \omega_c]) \\ 0 & (\xi_{\mathbf{k}}, \xi_{\mathbf{k}'} \notin [-\omega_c, \omega_c]) \end{cases}, \quad (2.6)$$

with a cutoff $\omega_c \ll \mu$ and $g, g' > 0$. Note that, under the condition $\omega_c \ll \mu$, the interaction affects only electrons on the “+” branch. Then the interaction term in the helicity representation is

$$\mathcal{H}_{\text{int}} \simeq -\frac{g}{4S} \sum_{\mathbf{k}, \mathbf{k}'} e^{i(\theta_{\mathbf{k}'} - \theta_{\mathbf{k}})} d_{-\mathbf{k}}^\dagger d_{\mathbf{k}}^\dagger d_{\mathbf{k}'} d_{-\mathbf{k}'}. \quad (2.7)$$

Here, we introduce an on-site TRS impurity scattering term as

$$\mathcal{H}_{\text{imp}} = \frac{u}{S} \sum_{i=1}^{N_i} \sum_{\mathbf{k}, \mathbf{k}'} e^{i(\mathbf{k}' - \mathbf{k}) \cdot \mathbf{R}_i} c^\dagger(\mathbf{k}) c(\mathbf{k}'), \quad (2.8)$$

where N_i is the number of the impurities in the system and \mathbf{R}_i ($i = 1, \dots, N_i$) is the impurity location. Then the impurity scattering term in the helicity representation is

$$H_{\text{imp}} = \frac{u}{S} \sum_{i=1}^{N_i} \sum_{\mathbf{k}, \mathbf{q}} e^{-i\mathbf{q} \cdot \mathbf{R}_i} P(\theta_{\mathbf{k}} - \theta_{\mathbf{k}+\mathbf{q}}) d_{\mathbf{k}+\mathbf{q}}^\dagger d_{\mathbf{k}}, \quad (2.9)$$

where $P(\theta) = \exp(i\theta/2) \cos(\theta/2)$ is a phase factor specific to Dirac electron systems. Here, $P(\pi) = 0$ means that the backscattering is forbidden. Moreover, this phase factor contributes to the π Berry phase, which leads to an antilocalization effect of single Dirac cone systems,²⁸ i.e., the electric conductivity in the system has a positive quantum correction.

We introduce a mean-field approximation in eq. (2.7) and construct a BCS mean-field Hamiltonian. By the BCS-type decoupling, a momentum-dependent pair potential $\Delta(\mathbf{k})$ is derived as

$$\Delta(\mathbf{k}) = \frac{g}{2S} e^{-i\theta_{\mathbf{k}}} \sum_{\mathbf{k}'} e^{i\theta_{\mathbf{k}'}} \langle d_{\mathbf{k}'} d_{-\mathbf{k}'} \rangle = \Delta e^{-i\theta_{\mathbf{k}}}, \quad (2.10)$$

and our interaction term is approximated as

$$\mathcal{H}_{\text{int}} \simeq -\frac{1}{2} \sum_{\mathbf{k}} \left[\Delta(\mathbf{k}) d_{-\mathbf{k}}^\dagger d_{\mathbf{k}}^\dagger + \Delta^*(\mathbf{k}) d_{\mathbf{k}} d_{-\mathbf{k}} \right]. \quad (2.11)$$

The pair potential in eq. (2.10) resembles a spinless chiral p -wave pair potential. This resemblance is related to the emergence of Majorana bound states around integer vortices.^{12,14} The difference between the two SCs is that the SC of helical Dirac electrons is time-reversal-symmetric, but the spinless p -wave SC is not.

In the representation of the original electrons operator c , this SC is composed of a mixture of s -wave (singlet) and p -wave (triplet) symmetries, and the interaction term is represented as

$$\mathcal{H}_{\text{int}} = -\sum_{\mathbf{k}} \sum_{s_1, s_2} \left[c_{-\mathbf{k}s_1}^\dagger \hat{\Delta}_{s_1 s_2}(\mathbf{k}) c_{\mathbf{k}s_2}^\dagger + h.c. \right], \quad (2.12)$$

where

$$\begin{aligned}\hat{\Delta}(\mathbf{k}) &= \hat{\Delta}_s(\mathbf{k}) + \hat{\Delta}_t(\mathbf{k}) \\ \hat{\Delta}_s(\mathbf{k}) &= \frac{\Delta}{2} \begin{pmatrix} 0 & 1 \\ -1 & 0 \end{pmatrix}, \\ \hat{\Delta}_t(\mathbf{k}) &= \frac{\Delta}{2} \begin{pmatrix} e^{-i\theta_{\mathbf{k}}} & 0 \\ 0 & -e^{i\theta_{\mathbf{k}}} \end{pmatrix}.\end{aligned}\quad (2.13)$$

Here, the s -wave pairing $\hat{\Delta}_s$ and the p -wave pairing $\hat{\Delta}_t$ are introduced. The mixture of two components originates from the broken inversion symmetry in the surface. The d vector corresponding to the triplet pairing component $\hat{\Delta}_t$ has a momentum dependence $\mathbf{d}(\mathbf{k}) \propto (k_x, k_y, 0)$, i.e., $\hat{\Delta}_t$ has a helical p -wave symmetry. Here, the helical p -wave SC is TRS p -wave SC, in which the chirality of the pair potential is different for each spin component.²⁹

By using the mean-field approximation in eq. (2.11), the Hamiltonian is approximated as

$$\begin{aligned}\mathcal{H} &\simeq \frac{1}{2} \Psi^\dagger \hat{H} \Psi \\ &= \frac{1}{2} \Psi^\dagger \left(\hat{H}_{\text{MF}} + \hat{V}_{\text{imp}} \right) \Psi \\ &= \frac{1}{2} \sum_{\mathbf{k}} \Psi^\dagger(\mathbf{k}) \hat{H}_{\text{MF}}(\mathbf{k}) \Psi(\mathbf{k}) \\ &\quad + \frac{1}{2} \frac{u}{S} \sum_{i=1}^{N_i} \sum_{\mathbf{k}, \mathbf{k}'} e^{i(\mathbf{k}' - \mathbf{k}) \cdot \mathbf{R}_i} \Psi^\dagger(\mathbf{k}) \hat{V}_1(\mathbf{k}, \mathbf{k}') \Psi(\mathbf{k}').\end{aligned}\quad (2.14)$$

We introduce a Nambu representation $\Psi(\mathbf{k}) = (\Psi_{\mathbf{k},e} \ \Psi_{\mathbf{k},h})^T \equiv (d_{\mathbf{k}} \ d_{-\mathbf{k}}^\dagger)^T$. The matrix elements in eq. (2.14) are defined as

$$\begin{aligned}\hat{H}_{\text{MF}}(\mathbf{k}) &= \begin{pmatrix} \xi_{\mathbf{k}} & \Delta e^{-i\theta_{\mathbf{k}}} \\ \Delta^* e^{i\theta_{\mathbf{k}}} & -\xi_{\mathbf{k}} \end{pmatrix}, \\ \hat{V}_1(\mathbf{k}, \mathbf{k}') &= \begin{pmatrix} P(\theta_{\mathbf{k}'} - \theta_{\mathbf{k}}) & 0 \\ 0 & -P(\theta_{-\mathbf{k}} - \theta_{-\mathbf{k}'}) \end{pmatrix}.\end{aligned}\quad (2.15)$$

We define an imaginary time Green's function as $\hat{G}(\tau) = -\langle T_\tau \Psi(\tau) \Psi^\dagger(0) \rangle$, where the time evolution of the operators $\Psi^{(\dagger)}$ is obtained from $\Psi^{(\dagger)}(\tau) = e^{\tau \mathcal{H}} \Psi^{(\dagger)} e^{-\tau \mathcal{H}}$. Then the Green's function in frequency space is $\hat{G}(i\omega_n) = \int_0^\beta d\tau e^{i\omega_n \tau} \hat{G}(\tau)$. From the equation of motion of the Green's function, the Gor'kov equation

$$(i\omega_n - \hat{H}) \hat{G}(i\omega_n) = \hat{1} \quad (2.16)$$

is derived, where $\omega_n = (2n+1)\pi T$ is the fermionic Matsubara frequency and T is the temperature.

When we assume that the scattering term \hat{V}_{imp} is perturbation using a perturbation series expansion with respect to u/S , the Green's function \hat{G} is represented as

$$\hat{G}(i\omega_n) = \hat{G}_0(i\omega_n) + \sum_{n=1}^{\infty} (\hat{G}_0(i\omega_n) \hat{V}_{\text{imp}})^n \hat{G}_0(i\omega_n), \quad (2.17)$$

where the nonperturbative Green's function $\hat{G}_0(i\omega_n) =$

$(i\omega_n - \hat{H}_{\text{MF}})^{-1}$ is introduced.

According to the AG theory, we perform the impurity average operation so that the system recovers its translational symmetry. By this operation, diagonal terms of momentum remain in the Hamiltonian and we only have to consider diagonal terms in the Green's function. By the impurity average operation, the quantity $\frac{1}{S} \sum_{i,j=1}^{N_i} e^{i(\mathbf{q} \cdot \mathbf{R}_i - \mathbf{q}' \cdot \mathbf{R}_j)}$ is replaced with $n_i \delta_{\mathbf{q}, \mathbf{q}'}$, where $n_i = N_i/S$ is the impurity concentration. We perform the impurity average of the right-hand side of eq. (2.17) for each term. The terms that correspond to $n = 1$ and $n = 2$ in eq. (2.17) are represented as diagrams in Figs. 1(a) and 1(b), respectively. They are the lowest-order terms about n_i . However, the term shown in Fig. 1(a) is negligible for the estimation of T_c because it just causes a constant self-energy shift and does not contribute to relaxation processes due to pair breaking.

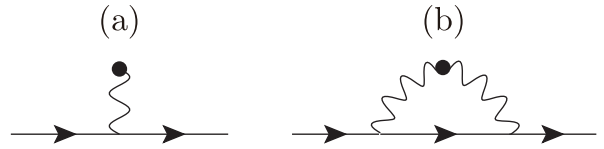


Fig. 1. Diagrams for self-energy terms of the lowest order in eq. (2.17). (a) and (b) correspond to $n = 1$ and $n = 2$, respectively. Wavy lines represent impurity scatterings.

Therefore, we consider the diagram in Fig. 1(b) and its higher-order series as the self-energy term for the estimation of T_c . The contribution of this term is $\mathcal{O}(n_i)$. We adopt this approximation following Abrikosov-Gor'kov²⁴ and Ambegaokar-Griffin.³⁰ Then the Green's function is calculated as

$$\begin{aligned}\hat{G}(\mathbf{k}, i\omega_n) &= \frac{1}{\left[\hat{G}_0(\mathbf{k}, i\omega_n) \right]^{-1} - \hat{\Sigma}(\mathbf{k}, i\omega_n)} \\ &= \frac{1}{i\tilde{\omega}_n - \hat{H}_{\text{MF}}(\mathbf{k}, i\omega_n)},\end{aligned}\quad (2.18)$$

where the self-energy term is

$$\begin{aligned}\hat{\Sigma}(\mathbf{k}, i\omega_n) &= \frac{n_i u^2}{S} \sum_{\mathbf{k}'} \hat{V}_1(\mathbf{k}, \mathbf{k}') \hat{G}(\mathbf{k}', i\omega_n) \hat{V}_1(\mathbf{k}', \mathbf{k}) \\ &= -\frac{n_i u^2}{S} \sum_{\mathbf{k}'} \frac{|P(\theta_{\mathbf{k}'} - \theta_{\mathbf{k}})|^2}{\tilde{\omega}_n^2 + |\tilde{\Delta}_n|^2 + \xi_{\mathbf{k}'}^2} \\ &\quad \times \begin{pmatrix} i\tilde{\omega}_n + \xi_{\mathbf{k}'} & -\tilde{\Delta}_n e^{-i\theta_{\mathbf{k}}} \\ -\tilde{\Delta}_n^* e^{i\theta_{\mathbf{k}}} & i\tilde{\omega}_n - \xi_{\mathbf{k}'} \end{pmatrix},\end{aligned}\quad (2.19)$$

and the renormalized mean-field Hamiltonian is

$$\hat{H}_{\text{MF}}(\mathbf{k}, i\omega_n) = \begin{pmatrix} \xi_{\mathbf{k}} & \tilde{\Delta}_n e^{-i\theta_{\mathbf{k}}} \\ \tilde{\Delta}_n^* e^{i\theta_{\mathbf{k}}} & -\xi_{\mathbf{k}} \end{pmatrix}. \quad (2.20)$$

In eqs. (2.18) -(2.20), $\tilde{\omega}_n$ and $\tilde{\Delta}_n$ are the renormalized frequency and pair potential, respectively.

By using eqs. (2.18) -(2.20), $\tilde{\omega}_n$ and $\tilde{\Delta}_n$ are self-

consistently calculated as

$$\tilde{\omega}_n = \omega_n + \frac{1}{2\tau_1} \frac{\tilde{\omega}_n}{\sqrt{\tilde{\omega}_n^2 + |\tilde{\Delta}_n|^2}}, \quad (2.21)$$

$$\tilde{\Delta}_n = \Delta + \frac{1}{2\tau_2} \frac{\tilde{\Delta}_n}{\sqrt{\tilde{\omega}_n^2 + |\tilde{\Delta}_n|^2}}, \quad (2.22)$$

where τ_1 and τ_2 are two types of relaxation times. In the case of the present SC, the two relaxation times are calculated as

$$\begin{aligned} \frac{1}{2\tau_1} &= \frac{1}{2\tau_2} = \pi n_i u^2 N_0 \int_0^{2\pi} \frac{d\theta}{2\pi} \cos^2(\theta/2) \\ &= \frac{\pi n_i u^2 N_0}{2}, \end{aligned} \quad (2.23)$$

where $N_0 = \frac{1}{S} \sum_{\mathbf{k}} \delta(\xi_{\mathbf{k}})$ is the density of states (DOS) at the Fermi energy. Therefore τ_1 and τ_2 are the same when considering $\mathcal{O}(n_i)$.

In order to estimate the order parameter or critical temperature, we need a self-consistent equation. A self-consistent equation is obtained using eq. (2.10):

$$\Delta = -\frac{g}{2\beta S} \sum_{i\omega_n} \sum_{\mathbf{k}} e^{i\theta_{\mathbf{k}}} G_{e,h}(\mathbf{k}, i\omega_n). \quad (2.24)$$

The self-consistent equation for the order parameter at zero temperature, Δ_0 , is

$$\Delta_0(n_i) = \frac{g}{2\beta S} \int_{-\omega_c}^{\omega_c} \frac{d\omega}{2\pi} \sum_{\mathbf{k}} \frac{\tilde{\Delta}}{\tilde{\omega}^2 + \xi_{\mathbf{k}}^2 + \tilde{\Delta}^2}, \quad (2.25)$$

where $\tilde{\omega} = \omega + \frac{1}{2\tau_1} \frac{\tilde{\omega}}{\sqrt{\tilde{\omega}^2 + |\tilde{\Delta}|^2}}$ and $\tilde{\Delta} = \Delta + \frac{1}{2\tau_2} \frac{\tilde{\Delta}}{\sqrt{\tilde{\omega}^2 + |\tilde{\Delta}|^2}}$.

On the other hand, the self-consistent equation for the mean-field critical temperature T_c is

$$1 = \frac{gT_c(n_i)}{2S} \sum_{i\omega_n} \sum_{\mathbf{k}} \frac{(2\tau_2 |\tilde{\omega}_n|)^{-1}}{\tilde{\omega}_n^2 + \xi_{\mathbf{k}}^2}. \quad (2.26)$$

Because the long-range SC order does not develop in 2D systems at a finite temperature, T_c calculated from the mean-field theory provides a criterion of the Berezinskii-Kosterlitz-Thouless (BKT) transition for the development of a quasi-long-range order.^{31,32}

By using the above equations, the values are obtained as

$$T_c(n_i) = T_c(0) - \frac{\pi}{4\tau_s(n_i)}, \quad T_c(0) = \frac{2e^\gamma}{\pi} \omega_c \exp\left(-\frac{2}{gN_0}\right), \quad (2.27)$$

$$\Delta_0(n_i) = \Delta_0(0) - \frac{\pi}{4\tau_s(n_i)}, \quad \Delta_0(0) = 2\omega_c \exp\left(-\frac{2}{gN_0}\right), \quad (2.28)$$

where the relaxation time τ_s is defined by

$$(\tau_s)^{-1} = (2\tau_1)^{-1} - (2\tau_2)^{-1}. \quad (2.29)$$

Because $(\tau_s)^{-1} = \mathcal{O}(n_i^2)$ is satisfied, T_c and Δ_0 do not decrease linearly in the present SC.

We compare this result with the results for other full-gap SCs reported in the literature^{23,24}. Table I shows

the results of the present SC in comparison with other 2D SCs. For each SC, $(2\tau_1)^{-1}$ and $(2\tau_2)^{-1}$ are calculated. We call SCs with $\tau_s^{-1} = \mathcal{O}(n_i^2)$ stable SCs, while SCs with $(\tau_s)^{-1} = \mathcal{O}(n_i)$ are fragile. In the table, ‘‘magnetic scattering’’ indicates that the impurity Hamiltonian takes a form as

$$\mathcal{H}_{\text{magimp}} = \frac{u}{S} \sum_{i=1}^{N_i} c_{n(i)}^\dagger \sigma_z c_{n(i)}, \quad (2.30)$$

which represents the scattering by magnetic impurities polarized along the z -direction. The forms of matrix elements for the BCS mean-field Hamiltonian $\hat{H}_{\text{MF}}(\mathbf{k})$ and the scattering Hamiltonian $\hat{V}_1(\mathbf{k}, \mathbf{k}')$ are also shown in the table.

Table I. Stability of SCs: (a) S -wave SC with TRS impurities. (b) S -wave SC with magnetic impurities. (c) Chiral p -wave SC with TRS impurities. (d) SC on TIs with TRS impurities. (e) SC on TIs with magnetic impurities.

	$\hat{H}_{\text{MF}}(\mathbf{k})$	$\hat{V}_1(\mathbf{k}, \mathbf{k}')$	stability
(a)	$\begin{pmatrix} \xi(\mathbf{k}) & \Delta \\ \Delta^* & -\xi_{\mathbf{k}} \end{pmatrix}$	$\begin{pmatrix} 1 & 0 \\ 0 & -1 \end{pmatrix}$	stable
(b)	$\begin{pmatrix} \xi(\mathbf{k}) & \Delta \\ \Delta^* & -\xi_{\mathbf{k}} \end{pmatrix}$	$\begin{pmatrix} 1 & 0 \\ 0 & 1 \end{pmatrix}$	fragile
(c)	$\begin{pmatrix} \xi(\mathbf{k}) & \Delta e^{-i\theta_{\mathbf{k}}} \\ \Delta^* e^{i\theta_{\mathbf{k}}} & -\xi_{\mathbf{k}} \end{pmatrix}$	$\begin{pmatrix} 1 & 0 \\ 0 & -1 \end{pmatrix}$	fragile
(d)	$\begin{pmatrix} \xi(\mathbf{k}) & \Delta e^{-i\theta_{\mathbf{k}}} \\ \Delta^* e^{i\theta_{\mathbf{k}}} & -\xi_{\mathbf{k}} \end{pmatrix}$	$\begin{pmatrix} P(\theta_{\mathbf{k}'} - \theta_{\mathbf{k}}) & 0 \\ 0 & -P(\theta_{-\mathbf{k}} - \theta_{-\mathbf{k}'}) \end{pmatrix}$	stable
(e)	$\begin{pmatrix} \xi(\mathbf{k}) & \Delta e^{-i\theta_{\mathbf{k}}} \\ \Delta^* e^{i\theta_{\mathbf{k}}} & -\xi_{\mathbf{k}} \end{pmatrix}$	$\begin{pmatrix} P(\theta_{\mathbf{k}'} - \theta_{\mathbf{k}} + \pi) & 0 \\ 0 & -P(\theta_{-\mathbf{k}} - \theta_{-\mathbf{k}'} + \pi) \end{pmatrix}$	fragile

To summarize this section, unconventional SCs induced by the s -wave attractive interaction on the surfaces of TIs are robust to TRS impurities. This result is achieved by calculating the dependences of T_c and Δ_0 on the TRS impurity concentration, where T_c provides a criterion of the BKT transition for a quasi-long-range order in 2D systems. The unconventional SC on the surface of TI is robust because of the cancellation of two phase factors, one from the pairing potential and the other arising when a Dirac electron is scattered by a TRS impurity. In contrast, unconventional SCs reported in the literature, such as the d -wave and chiral p -wave SCs,^{20–23} are sensitively suppressed through scattering by a tiny concentration of impurities because of the phase factor of the pairing potential.

We treated impurities as perturbations in this section. The perturbation theory is valid if $u^2 n_i N_0$ is much smaller than the pair potential Δ though a rough estimate. This estimation is derived from the reduction in the pair potential due to magnetic scattering.

3. Nonperturbative Approach

3.1 Model and method

In order to study the impurity effects on the SC on the surfaces of TIs by real-space BdG calculation, we use a tight-binding model of Bi₂Se₃ in slab geometry, which is an effective model of 3D TI.^{26,27} We obtain a single Dirac cone on the surface of the slab.

In order to study impurity effects, we consider a Hamiltonian composed of three terms in the same way as in §2:

$$\mathcal{H} = \mathcal{H}_0 + \mathcal{H}_{\text{int}} + \mathcal{H}_{\text{imp}}. \quad (3.1)$$

Here, \mathcal{H}_0 is the effective tight-binding Hamiltonian of Bi₂Se₃, which is first introduced by Zhang *et al.*²⁶ On the other hand, \mathcal{H}_{int} is the interaction term and \mathcal{H}_{imp} is the impurity potential.

The Hamiltonian \mathcal{H}_0 has a structure of a 4×4 matrix, because of the presence of two orbitals and spin indices. The two orbitals are the antibonding and bonding orbitals constructed from the p_z -orbitals of Bi and Se atoms; they have different parities from each other. We refer to these orbitals as “ E ” and “ H ” orbitals, respectively. Bi₂Se₃ has a rhombohedral symmetry, but for simplicity we adopt a model reduced to the D_{4h} symmetry.²⁶ In studying fundamental properties of SSs near the Dirac point, this approximation is valid since anisotropy owing to the rhombohedral symmetry is weak near the Dirac point.

A Bloch representation of \mathcal{H}_0 ²⁶ is

$$\hat{H}_0(\mathbf{k}) = \begin{pmatrix} \epsilon_{\mathbf{k}} + M_{\mathbf{k}} & A_z k_z & 0 & A_{\parallel} k_{-} \\ A_z k_z & \epsilon_{\mathbf{k}} - M_{\mathbf{k}} & A_{\parallel} k_{-} & 0 \\ 0 & A_{\parallel} k_{+} & \epsilon_{\mathbf{k}} + M_{\mathbf{k}} & -A_z k_z \\ A_{\parallel} k_{+} & 0 & -A_z k_z & \epsilon_{\mathbf{k}} - M_{\mathbf{k}} \end{pmatrix}, \quad (3.2)$$

where

$$\mathcal{H}_0 = \sum_{\mathbf{k}} c^{\dagger}(\mathbf{k}) \hat{H}_0(\mathbf{k}) c(\mathbf{k}), \quad c(\mathbf{k}) = (c_{\mathbf{k}\uparrow E} \ c_{\mathbf{k}\uparrow H} \ c_{\mathbf{k}\downarrow E} \ c_{\mathbf{k}\downarrow H})^T, \quad \mathcal{H}_{\text{imp}}.$$

$$\epsilon_{\mathbf{k}} = D_{\parallel} k_{\parallel}^2 + D_z k_z^2,$$

$$M_{\mathbf{k}} = M - B_{\parallel} k_{\parallel}^2 - B_z k_z^2 \quad (B_{\parallel}, B_z < 0),$$

$$k_{\pm} = k_x \pm i k_y, \mathbf{k}_{\parallel} = (k_x, k_y),$$

where A_{\parallel} and A_z represent the strength of SOIs, while M is the energy difference between the two orbitals. The band curvatures of the two subbands are different, which arises from nonzero B_{\parallel} and B_z . Here, we note that, due to the gauge transformation defined in eq. (18) of ref. 27, $\hat{H}_0(\mathbf{k})$ is not invariant under the operation of a standard choice for the time reversal operator, $I \otimes i \sigma_y \cdot \mathcal{K}$, where I is the identity matrix acting on subband indices, σ_y is the Pauli matrix acting on the spin indices, and \mathcal{K} is the complex conjugate operator.

In order to construct a Wannier representation of \mathcal{H}_0 , we perform a substitution such that

$$k_i \rightarrow \sin k_i, k_i^2 \rightarrow 2 - 2 \cos k_i \quad (i = x, y, z),$$

and the Fourier transformation

$$c(\mathbf{k}) = \frac{1}{\sqrt{N_x N_y N_z}} \sum_{x=1}^{N_x} \sum_{y=1}^{N_y} \sum_{z=1}^{N_z} e^{i\mathbf{k} \cdot \mathbf{r}} c(\mathbf{r}), \quad (3.3)$$

$$c^{\dagger}(\mathbf{k}) = \frac{1}{\sqrt{N_x N_y N_z}} \sum_{x=1}^{N_x} \sum_{y=1}^{N_y} \sum_{z=1}^{N_z} e^{-i\mathbf{k} \cdot \mathbf{r}} c^{\dagger}(\mathbf{r}). \quad (3.4)$$

For simplicity, we choose the model parameters in eq. (3.2) as

$$\begin{aligned} A_x &= 1 \text{ eV}, A_z = 0.5 \text{ eV}, B_x = 1.5 \text{ eV}, B_z = 0.3 \text{ eV}, \\ D_x &= D_z = 0, M = 0.5 \text{ eV}, \end{aligned} \quad (3.5)$$

where the particle-hole symmetry about subbands E and H is imposed. We assume that the lattice parameter is normalized as 1. Then the curvatures of two subbands are equivalent except signs. For readers, we cite the parameters given by *ab initio* calculations²⁶ below:

$$\begin{aligned} A_x &= 0.5 \text{ eV}, A_z = 0.2 \text{ eV}, B_x = 0.6 \text{ eV}, B_z = 0.1 \text{ eV}, \\ D_x &= 0.1 \text{ eV}, D_z = 0.05 \text{ eV}, M = 0.3 \text{ eV}. \end{aligned} \quad (3.6)$$

We obtain a single Dirac cone at the Γ point in a surface by considering a slab geometry when the parameters support nontrivial Z_2 topological indices. In this paper, we impose an open boundary condition in the z -direction and periodic boundary conditions in the x - and y -directions. Figure 2 shows energy dispersions for \mathcal{H}_0 . In the dispersion, gapless SSs exist inside the bulk band gap.

Then, we introduce the s -wave attractive interaction term \mathcal{H}_{int} as

$$\mathcal{H}_{\text{int}} = -\frac{1}{2} \sum_{i,j,\sigma,\sigma',\tau,\tau'} c_{i\tau\sigma}^{\dagger} c_{j\tau'\sigma'}^{\dagger} g_{\sigma\sigma'}^{\tau\tau'}(i,j) c_{j\tau'\sigma'} c_{i\tau\sigma}, \quad (3.7)$$

where $g_{\sigma\sigma'}^{\tau\tau'}(i,j) = g_{\sigma'\sigma}^{\tau'\tau}(j,i)$ holds.

As the third term of our model Hamiltonian, we introduce the s -wave TRS impurity scattering Hamiltonian \mathcal{H}_{imp} . The impurity scattering Hamiltonian \mathcal{H}_{imp} is rep-

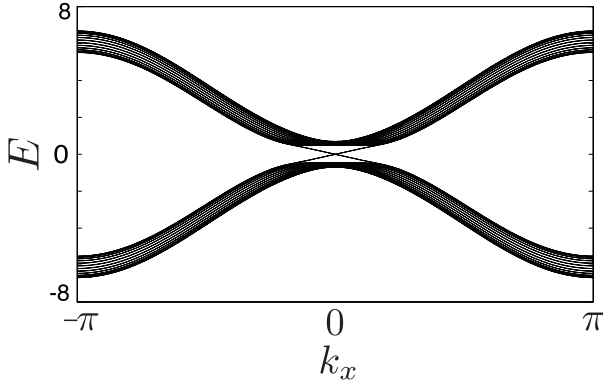


Fig. 2. Dispersion when the set of Hamiltonian parameters is $A_x = 1$ eV, $A_z = 0.5$ eV, $B_x = 1.5$ eV, $B_z = 0.3$ eV, $D_x = D_z = 0$ and $M = 0.5$ eV. An open-boundary condition is imposed in the z -direction and $N_z = 12$. We show the case of $k_y = 0$.

resented as

$$\mathcal{H}_{\text{imp}} = u \sum_{i=1}^{N_i} c_{n(i)}^\dagger c_{n(i)} = c^\dagger \hat{H}_{\text{imp}} c, \quad (3.8)$$

where N_i is the number of impurities, $n(i)$ is the location of the i -th impurity, u is the strength of the impurity potential, and \hat{H}_{imp} is the matrix representation of the Hamiltonian.

By solving the BdG equation for the introduced model Hamiltonian, we analyze the impurity effects on the SC on the surfaces of TIs. To construct the BdG equation, we perform the mean-field approximation

$$\begin{aligned} & c_{i\tau\sigma}^\dagger c_{j\tau'\sigma'}^\dagger c_{j\tau'\sigma'} c_{i\tau\sigma} \\ \rightarrow & \langle c_{i\tau\sigma}^\dagger c_{j\tau'\sigma'}^\dagger \rangle c_{j\tau'\sigma'} c_{i\tau\sigma} + c_{i\tau\sigma}^\dagger c_{j\tau'\sigma'}^\dagger \langle c_{j\tau'\sigma'} c_{i\tau\sigma} \rangle \\ & - \langle c_{i\tau\sigma}^\dagger c_{j\tau'\sigma'}^\dagger \rangle \langle c_{j\tau'\sigma'} c_{i\tau\sigma} \rangle, \end{aligned} \quad (3.9)$$

which leads to the BCS mean-field Hamiltonian

$$\mathcal{H} \simeq \frac{1}{2} \Psi^\dagger \hat{H}_{\text{MF}} \Psi, \quad (3.10)$$

where $\Psi = (\Psi_e \ \Psi_h)^T = (c \ [c^\dagger]^T)^T$ is a Nambu spinor and

$$\begin{aligned} \hat{H}_{\text{MF}} = & \begin{pmatrix} \hat{H}_0 + \hat{H}_{\text{imp}} + \mu \hat{I} & \hat{\Delta} \\ \hat{\Delta}^\dagger & -[\hat{H}_0 + \hat{H}_{\text{imp}} + \mu \hat{I}]^T \end{pmatrix} \\ & + E_\Delta \begin{pmatrix} \hat{I} & 0 \\ 0 & \hat{I} \end{pmatrix} \end{aligned} \quad (3.11)$$

is the matrix element. Here, μ is the Fermi energy, E_Δ is a constant energy shift, and \hat{I} is the identity matrix. The constant energy shift E_Δ originates from the terms like $\langle cc \rangle \langle c^\dagger c^\dagger \rangle$ in eq. (3.9) and calculated as $E_\Delta = \sum_{ij\sigma\sigma'\tau\tau'} g_{\sigma\sigma'}^{\tau\tau'} \langle c_{i\tau\sigma}^\dagger c_{j\tau'\sigma'}^\dagger \rangle \langle c_{j\tau'\sigma'} c_{i\tau\sigma} \rangle$. Since the contribution of this term is just a constant energy shift, we are able to neglect this term in determining the mean-field self-consistently. In eq. (3.11), the pair potential is introduced as

$$\Delta_{\sigma\sigma'}^{\tau\tau'}(i, j) = g_{\sigma\sigma'}^{\tau\tau'}(i, j) \langle c_{i\tau\sigma} c_{j\tau'\sigma'} \rangle. \quad (3.12)$$

The 4×4 pair potential matrix $\hat{\Delta}$ is expressed as

$$\hat{\Delta} = \begin{pmatrix} \Delta_{\uparrow\uparrow}^{EE} & \Delta_{\uparrow\uparrow}^{EH} & \Delta_{\uparrow\downarrow}^{EE} & \Delta_{\uparrow\downarrow}^{EH} \\ \Delta_{\uparrow\downarrow}^{EH} & \Delta_{\uparrow\downarrow}^{HH} & \Delta_{\uparrow\downarrow}^{HE} & \Delta_{\uparrow\downarrow}^{HH} \\ \Delta_{\downarrow\uparrow}^{EE} & \Delta_{\downarrow\uparrow}^{EH} & \Delta_{\downarrow\downarrow}^{EE} & \Delta_{\downarrow\downarrow}^{EH} \\ \Delta_{\downarrow\uparrow}^{EH} & \Delta_{\downarrow\uparrow}^{HH} & \Delta_{\downarrow\downarrow}^{HE} & \Delta_{\downarrow\downarrow}^{HH} \end{pmatrix}. \quad (3.13)$$

Note that $\Delta_{\sigma\sigma'}^{\tau\tau'}(i, j) = -\Delta_{\sigma'\sigma}^{\tau'\tau}(j, i)$ is satisfied because of the Pauli exclusion principle.

By diagonalizing \hat{H}_{MF} , we obtain the excitation energy spectrum of the Bogoliubov quasiparticles E_ν and the set of eigenvectors $w_\nu(i\tau\sigma r)$ corresponding to amplitudes of the quasiparticle wave functions, that is,

$$\hat{H}_{\text{MF}} w_\nu = E_\nu w_\nu. \quad (3.14)$$

The indices i , τ , σ , and r represent the site, subbands, spin, and particle-hole indices, respectively.

The mean-field Hamiltonian has the particle-hole symmetry (PHS), i.e.

$$\{\hat{C}, \hat{H}_{\text{MF}}\} = 0, \quad (3.15)$$

where $\hat{C} = \hat{r}_x \hat{K}$ and \hat{r}_x transforms a particle and a hole each other by the Pauli operator in the particle hole space and \hat{K} is the complex conjugate operator. Then w_ν and $\hat{C}w_\nu$ are referred to as a particle-hole pair, i.e., $\hat{H}_{\text{MF}} \hat{C}w_\nu = -E_\nu \hat{C}w_\nu$ is satisfied. For convenience, we redefine the index ν of an eigenvalue so that w_ν and $w_{-\nu}$ are a particle-hole pair, where $\nu > 0$ and $E_\nu > 0$. Then, $w_{-\nu} = \hat{C}w_\nu$ and $E_{-\nu} = -E_\nu$ hold.

Then we introduce the creation and annihilation operators of quasiparticles, α_ν . Here, Ψ and α_ν are related by the Bogoliubov transformation

$$\Psi = \sum_\nu w_\nu \alpha_\nu = \sum_{\nu>0} (w_\nu \alpha_\nu + w_{-\nu} \alpha_\nu^\dagger), \quad (3.16)$$

and its inverse transformation

$$\alpha_\nu = w_\nu^T \Psi, \quad \alpha_\nu^\dagger = w_{-\nu}^T \Psi. \quad (3.17)$$

The relation $\alpha_{-\nu} = \alpha_\nu^\dagger$ holds because of PHS. Bogoliubov quasiparticles obey commutation relations of fermions so that $\{\alpha_\nu, \alpha_\mu^\dagger\} = \delta_{\nu,\mu}$ and $\{\alpha_\nu, \alpha_\mu\} = 0$ are satisfied. The mean-field Hamiltonian is diagonalized as

$$\mathcal{H} = \frac{1}{2} \sum_{\nu>0} E_\nu (\alpha_\nu^\dagger \alpha_\nu - \alpha_\nu \alpha_\nu^\dagger). \quad (3.18)$$

In order to calculate the pair potential, we introduce an imaginary time Green's function, $\hat{G}(\tau) = -\langle T_\tau \Psi(\tau) \Psi^\dagger(0) \rangle$. By the Bogoliubov transformation, the Green's function is expressed in the quasiparticle representation

$$\hat{G}(\tau) = - \sum_\nu w_\nu w_\nu^T \langle T_\tau \alpha_\nu(\tau) \alpha_\nu^\dagger \rangle. \quad (3.19)$$

The pair potential defined in eq. (3.12) is calculated from the anomalous part of the Green's function, i.e.,

$$\begin{aligned} \Delta_{\sigma\sigma'}^{\tau\tau'}(i, j) &= -g_{\sigma\sigma'}^{\tau\tau'}(i, j) G_{i\tau\sigma e, j\tau'\sigma' h}(\tau = +0) \\ &= g_{\sigma\sigma'}^{\tau\tau'}(i, j) \sum_{\nu>0} \{ [1 - f(E_\nu)] u_\nu(i\tau\sigma) v_\nu^*(j\tau'\sigma') \\ &\quad + f(E_\nu) v_\nu^*(i\tau\sigma) u_\nu(j\tau'\sigma') \}, \end{aligned} \quad (3.20)$$

where the two vectors u and v are introduced:

$$u_\nu(i\tau\sigma) = w_\nu(i\tau\sigma e), v_\nu(i\tau\sigma) = w_\nu(i\tau\sigma h). \quad (3.21)$$

Here, u_ν and v_ν correspond to the amplitudes of the particle and hole wave functions, respectively. In eq.(3.20), $f(E) = (e^{\beta E} + 1)^{-1}$ is the Fermi-Dirac distribution function. Note that $u_\nu^* = v_{-\nu}$ is satisfied because of PHS.

3.2 Symmetry of the order parameter

We first consider the impurity-free case and this subsection is devoted to remarks satisfied in the absence of impurities. We analyze the order parameter, which is determined from the real-space BdG equation eq. (3.20). In this subsection, we concentrate on the order parameter $\hat{\Delta}$, which does not contain the interaction coefficients $g_{\sigma\sigma'}^{\tau\tau'}(i, j)$ introduced in eq. (3.7):

$$\hat{\Delta}_{\sigma\sigma'}^{\tau\tau'}(i, j) \equiv \langle c_{i\tau\sigma} c_{j\tau'\sigma'} \rangle. \quad (3.22)$$

This order parameter $\hat{\Delta}$ represents the superfluid density.

The interaction parameter in eq. (3.7) is

$$g_{\uparrow\downarrow}^{EE}(i, i) = g_{\downarrow\uparrow}^{EE}(i, i) = g_{\uparrow\downarrow}^{HH}(i, i) = g_{\downarrow\uparrow}^{HH}(i, i) = 2 \text{ eV}; \quad (3.23)$$

for the other components, $g_{\sigma\sigma'}^{\tau\tau'}(i, j) = 0$. By choosing the interaction coefficients as in eq. (3.23), we only consider onsite attractive interactions between electrons in the same subband. We take the system size as $N_x = N_y = 20$ and $N_z = 8$ in this subsection.

First, we show the onsite components $\hat{\Delta}(i, i)$ of the order parameter obtained using the BdG equation. For the onsite component, the result of the calculation is

$$\hat{\Delta}(i, i) = \begin{pmatrix} 0 & 0 & \eta_1(z) & i\eta_2(z) \\ 0 & 0 & -i\eta_2(z) & \eta_3(z) \\ -\eta_1(z) & i\eta_2(z) & 0 & 0 \\ -i\eta_2(z) & -\eta_3(z) & 0 & 0 \end{pmatrix},$$

$$\eta_1(1) = 1.45 \times 10^{-3}, \eta_2(1) = 1.35 \times 10^{-3},$$

$$\eta_3(1) = 1.05 \times 10^{-3}. \quad (3.24)$$

where η_1 and η_3 are even functions of z , while η_2 is an odd function of z with the symmetry center at $z = 4.5$, i.e., the relations $\eta_1(z) = \eta_1(9 - z)$, $\eta_2(z - 9) = -\eta_2(9 - z)$, and $\eta_3(z - 9) = \eta_3(9 - z)$ hold. The amplitude of each η decreases when z is nearer to the symmetry center, for example, $\eta_1(1) = 1.45 \times 10^{-3}$, $\eta_1(2) = 3.05 \times 10^{-4}$, $\eta_1(3) = 2.39 \times 10^{-5}$, $\eta_1(4) = 1.30 \times 10^{-6}$; therefore

$$\eta_1(1) > \eta_1(2) > \eta_1(3) > \eta_1(4),$$

holds. This amplitude dependences on z imply that the Cooper pairings are mainly formed from the helical Dirac electrons, which are localized at the surface. Since $\hat{\Delta}(i, i)$ is an antisymmetric matrix, each onsite order parameter η is a singlet component. Here, $\hat{\Delta}(i, i)$ is independent of x and y because of translational symmetry.

Then, we show a part of the off-site components $\hat{\Delta}(i, i + e_x)$ of the order parameter obtained using the BdG equation. Here, $\hat{\Delta}(i, i + e_x)$ represents the coherence between the two sites neighboring in the x -direction. The

result of the calculation is

$$\hat{\Delta}(i, i + e_x) = \begin{pmatrix} -\eta'_1(z) & i\eta'_2(z) & \eta'_3(z) & i\eta'_4(z) \\ i\eta'_2(z) & \eta'_5(z) & -i\eta'_4(z) & \eta'_6(z) \\ -\eta'_3(z) & i\eta'_4(z) & -\eta'_1(z) & -i\eta'_2(z) \\ -i\eta'_4(z) & -\eta'_6(z) & -i\eta'_2(z) & \eta'_5(z) \end{pmatrix},$$

$$\eta'_1(1) = 1.63 \times 10^{-4}, \eta'_2(1) = 1.71 \times 10^{-4},$$

$$\eta'_3(1) = 1.18 \times 10^{-3}, \eta'_4(1) = 1.02 \times 10^{-3},$$

$$\eta'_5(1) = 1.60 \times 10^{-4}, \eta'_6(1) = 1.12 \times 10^{-3}, \quad (3.25)$$

where η'_2 , η'_3 , and η'_6 are even functions of z , while η'_1 , η'_4 , and η'_5 are odd functions of z with the symmetry center at $z = 4.5$. Since η'_1 , η'_2 , and η'_5 are symmetric components of the above matrix, they are triplet components. In contrast, η'_3 , η'_4 , and η'_6 are antisymmetric components of the matrix and are singlet components.

The above results support the notion that an onsite s -wave interaction induces the order parameter with a mixture of singlet and triplet components, which agrees with the results of the idealistic helical Dirac electron model in §2.

Generally, the order parameter is written as

$$\hat{\Delta}(x, y, z; x + t_x e_x, y + t_y e_y, z) = A(t, z)(t_x I \otimes I - t_y I \otimes (i\sigma_z)) + B(t, z)(t_x \tau_z \otimes I - t_y \tau_z \otimes (i\sigma_z)) + C(t, z)(t_x \tau_x \otimes (-i\sigma_z) - t_y \tau_x \otimes I) + D(t, z)I \otimes (i\sigma_y) + E(t, z)\tau_z \otimes (i\sigma_y) + F(t, z)\tau_y \otimes \sigma_x, \quad (3.26)$$

where $t = \sqrt{t_x^2 + t_y^2}$. The above results are in the case of $t_x = t_y = 0$ and $t_x = 1, t_y = 0$. Here, C , D , and E are even functions, while A , B , and F are odd functions of z . In the above equation, σ acts on the spin basis and the pseudospin Pauli matrix τ acts on the basis of E and H subbands.

According to the transformation rule in Appendix 1, the order parameter of the form in eq. (3.26) is invariant under a set of symmetry operations that belong to D_{4h} . Since the noninteracting original Hamiltonian is invariant under the symmetry operations in D_{4h} , the invariance of the order parameter under the operation indicates that the SC realized in the model breaks no additional spatial symmetries.

3.3 Stability against impurities

Now, we analyze the impurity concentration and impurity strength dependences of the pair potential for the tight-binding model of Bi_2Se_3 . We assume that impurities are located on one of the two surfaces. We concentrate on a pair potential on a surface with impurities. We define a surface with impurities as $z = 1$.

By using the method of efficiently compensating for the change in the density of states (DOS) explained in §A.3 in the case of the reference systems, we analyze the impurity concentration dependence of the pair potential of Bi_2Se_3 . Here, note that there are 16 components in

the BdG equation for Bi_2Se_3 . Therefore, one might speculate that the method of compensating for the change in the DOS for the BdG equation is complicated. However, by choosing the Hamiltonian parameters used in §3.2, we can focus on $\Delta_{\uparrow\downarrow}^{EE}$ and $\Delta_{\uparrow\downarrow}^{HH}$. This is because we only consider onsite attractive interactions between electrons in the same subband. In the following discussion, we concentrate on the dependences of $\Delta_{\uparrow\downarrow}^{EE}$ on the scattering strength and impurity concentration, and $\Delta_{\uparrow\downarrow}^{EE}$ is written as Δ .

In order to describe the behavior of the pair potential purely due to relaxation processes, we concentrate on the value

$$1 + \frac{\delta\Delta(u, n_i)}{\Delta_0} = \frac{\langle\langle\Delta(u, n_i)\rangle_x\rangle_{\text{imp}}}{\langle\Delta_{\text{(DOS)}}(u, n_i)\rangle_{\text{imp}}}, \quad (3.27)$$

which represents the relative value of the pair potential due to the relaxation. In eq. (3.27), the quantities Δ_0 , $\delta\Delta$, $\Delta(u, n_i)$, and $\Delta_{\text{(DOS)}}(u, n_i)$ represent the impurity-free pair potential, the change in pair potential purely due to the relaxation, the result of the BdG calculation, and the relaxation-ignored pair potential, respectively. The definitions of these quantities are introduced in §A.3. Note that $\Delta(u, n_i)$ depends on the site and impurity configuration, and $\Delta_{\text{(DOS)}}(u, n_i)$ depends on the impurity configuration. Moreover, $\langle\cdots\rangle_x$ and $\langle\cdots\rangle_{\text{imp}}$ represent the average over sites and impurity configuration, respectively, whose definitions are given in §A.3.

In the model, we estimate $\Delta_{\text{(DOS)}}$ as

$$\Delta_{\text{(DOS)}}(u, n_i) = \Delta_0 \times \frac{\left[\sum_{\nu} \frac{\Delta_{\text{(DOS)}}(u, n_i)}{\sqrt{E_{\nu}(u, n_i)^2 + \Delta_{\text{(DOS)}}(u, n_i)^2}} \rho(E_{\nu}(u, n_i), z = 1) \right]}{\left[\sum_{\nu} \frac{\Delta_0}{\sqrt{E_{0\nu}^2 + \Delta_0^2}} \rho^{(0)}(E_{0\nu}, z = 1) \right]}, \quad (3.28)$$

where $\rho^{(0)}(E, z = 1)$ is the DOS at the surface without impurities, while $\rho(E, z = 1)$ is that with impurities. Here, $E_{0\nu}$ and $E_{\nu}(u, n_i)$ represent the energy spectra without and with impurities, respectively. We note that $E_{\nu}(u, n_i)$ depends on the impurity configuration.

We show the results of $1 + \delta\Delta(u, n_i)/\Delta_0$ in Figs. 3 and 4. Figure 3 shows the impurity concentration dependence of the pair potential for the TRS impurities. In the figure, the results for the scattering strength of the choices $u = 0.1$ and $u = 20$ are plotted.

For $u = 0.1$, the inset in Fig. 3 shows that the reduction in the pair potential is proportional to the square of the impurity concentration, i.e., $\propto n_i^2$ for small n_i . Since the order of the pair potential is 10^{-3} , $u = 0.1$ is much larger than the pair potential. Therefore, it is beyond the applicability of the AG theory. The robustness of the SC obtained in the BdG calculation indicates the stability of the SC beyond the perturbative range. For $u = 0.1$, the pair potential vanishes at $n_i \simeq 5\%$. On the other hand, when the strength of impurity potential is $u = 20$, which indicates a strong impurity potential regarded practically as a lattice defect, the pair potential vanishes at $n_i \simeq 4\%$.

In Fig. 4, we compare the results for TRS scattering with magnetic scattering. In the case of magnetic scattering, the pair potential decreases linearly for small concentrations. We find that the reduction rate of the pair potential depends on the direction along x or z of the magnetization for magnetic impurities. We deduce that a difference between the two directions remains even at an impurity concentration range higher than 0.25% in spite of the large error bars. In fact, the difference in the impurity concentration dependences at 0.25% is reliable and statistically meaningful. Actually, according to the AG theory, the reduction rates of the pair potential are the same in both cases. Therefore, a difference in the impurity concentration dependence arises from higher-order perturbations. This difference is mainly caused by the difference in the change in DOS, which depends on the polarization.³³

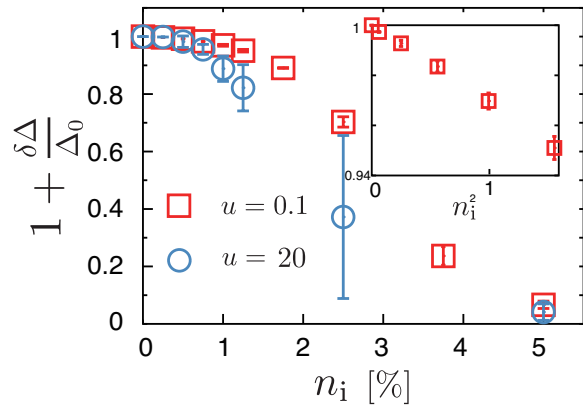


Fig. 3. (Color online) Impurity concentration dependence of pair potential for TRS scattering. The abscissa represents the impurity concentration n_i , while the ordinate represents $1 + \delta\Delta(u, n_i)/\Delta_0$. In the calculation, we fix the system size at $N_x N_y = 400$. The squares and circles illustrate the results for scatterings of strength $u = 0.1$ and $u = 20$, respectively. In the inset, the same quantity $1 + \delta\Delta(u, n_i)/\Delta_0$ is plotted as a function of the square of the impurity concentration n_i^2 for $u = 0.1$.

3.4 Spatial structure

In this section, we analyze spatial structures induced by an impurity. We focus on the spatial structures of the pair potential and wave functions of Bogoliubov quasiparticles. To study the pair potential, we obtain a configuration of induced currents around an impurity. To study wave functions of quasiparticles, we analyze the properties of bound states around an impurity. Here, we assume that the impurity is located at $(x, y) = (0, 0)$ and that the impurity potential u is strong.

In the calculation, we choose the parameters of \mathcal{H} as

$$A_x = 1 \text{ eV}, A_z = 0.5 \text{ eV}, B_x = 1.5 \text{ eV}, B_z = 0.3 \text{ eV}, \\ D_x = D_z = 0, M = 0.5 \text{ eV}, \quad (3.29)$$

$$g_{\sigma\sigma'}^{\tau\tau'}(\mathbf{r}, \mathbf{r}) = 2 \text{ eV} \quad (\text{onsite components}), \quad (3.30)$$

$$g_{\sigma\sigma'}^{\tau\tau'}(\mathbf{r}, \mathbf{r}') = 1 \text{ eV} \quad (\mathbf{r} \text{ and } \mathbf{r}' \text{ are the nearest neighbors}).$$

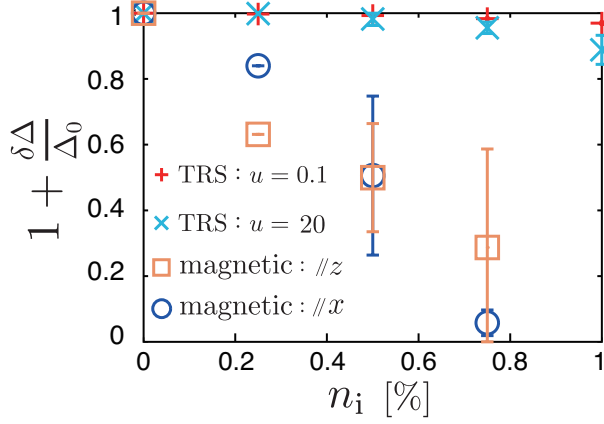


Fig. 4. (Color online) Impurity concentration dependence of pair potential for TRS and magnetic impurity scatterings. The abscissa represents the impurity concentration n_i , while the ordinate represents $1 + \delta\Delta(u, n_i)/\Delta_0$. In the calculation, we fix the system size at $N_x N_y = 400$. The plus and cross illustrate the results for the TRS impurity scattering when $u = 0.1$ and $u = 20$, respectively. The squares and circles illustrate the results for the magnetic impurity scattering, which were polarized along the x - and z -directions.

(3.31)

We take the system size as $N_x = N_y = 20$ and $N_z = 8$.

First, we show the spatial dependence of the onsite s -wave components around the impurity. Here, s -wave components are defined as

$$\begin{aligned}\Delta_{\uparrow\downarrow s}^{\tau\tau'}(\mathbf{r}) &\equiv \Delta_{\uparrow\downarrow}^{\tau\tau'}(\mathbf{r}, \mathbf{r}) \\ \Delta_{\downarrow\uparrow s}^{\tau\tau'}(\mathbf{r}) &\equiv \Delta_{\downarrow\uparrow}^{\tau\tau'}(\mathbf{r}, \mathbf{r}).\end{aligned}\quad (3.32)$$

Figure 5 shows the spatial dependence of one of those components $\Delta_{\uparrow\downarrow s}^{EE}(\mathbf{r})$. The amplitude of $\Delta_{\uparrow\downarrow s}^{EE}(\mathbf{r})$ nearly vanishes at the impurity site. This is because the impurity potential is so strong that it is nearly regarded as a lattice defect and the electron density is extremely small at the impurity site.

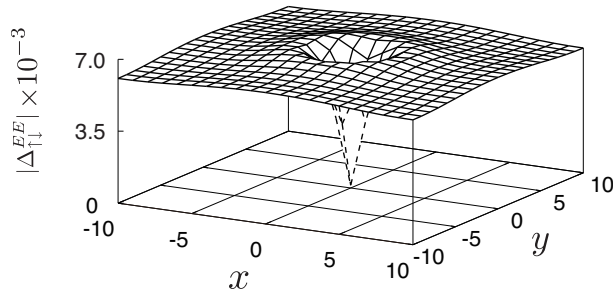


Fig. 5. Spatial dependence of $|\Delta_{\uparrow\downarrow}^{EE}|$.

We then show the spatial dependence of the onsite p -wave components. Figure 6 shows $\Delta_{\uparrow\uparrow p}^{EH}(\mathbf{r}) \equiv \Delta_{\uparrow\uparrow}^{EH}(\mathbf{r}, \mathbf{r})$ which is one of the onsite p -wave components. This component reflects the existence of inter-orbital Cooper pairings. At the impurity site, this value is zero in agreement with the symmetry of the original Hamilto-

nian with an impurity potential. Because the system has the C_4 rotational symmetry around the impurity site, the impurity site is a singular point of the vector field, $(\text{Re}[\Delta_{\uparrow\uparrow p}^{EH}(\mathbf{r})], \text{Im}[\Delta_{\uparrow\uparrow p}^{EH}(\mathbf{r})])$, where $\Delta_{\uparrow\uparrow p}^{EH}(\mathbf{r})$ is zero. Without the impurity, this component vanishes because the lattice translational symmetries along the x - and y -directions exist and every site is the rotational center.

Figure 7 shows the spatial configurations of two normalized vector fields, $\mathbf{F}_{\uparrow\uparrow}^{EH}(\mathbf{r})/|\mathbf{F}_{\uparrow\uparrow}^{EH}(\mathbf{r})|$ and $\mathbf{F}_{\downarrow\downarrow}^{EH}(\mathbf{r})/|\mathbf{F}_{\downarrow\downarrow}^{EH}(\mathbf{r})|$, where

$$\mathbf{F}_{\uparrow\uparrow}^{EH}(\mathbf{r}) = (\text{Re}[\Delta_{\uparrow\uparrow p}^{EH}(\mathbf{r})], \text{Im}[\Delta_{\uparrow\uparrow p}^{EH}(\mathbf{r})]), \quad (3.33)$$

and

$$\mathbf{F}_{\downarrow\downarrow}^{EH}(\mathbf{r}) = (\text{Re}[\Delta_{\downarrow\downarrow p}^{EH}(\mathbf{r})], \text{Im}[\Delta_{\downarrow\downarrow p}^{EH}(\mathbf{r})]). \quad (3.34)$$

Since we fix the length of the arrows representing the vector fields, only the directions of the arrows are meaningful, which correspond to the complex phases of $\Delta_{\uparrow\uparrow p}^{EH}(\mathbf{r})$ or $\Delta_{\downarrow\downarrow p}^{EH}(\mathbf{r})$. At singular points, where $|\mathbf{F}| = \vec{0}$ holds, the arrows are not plotted. In each component, there exist vortices at $(0, 0)$, $(0, 10)$, $(10, 0)$, and $(10, 10)$. In the $\Delta_{\uparrow\uparrow}^{EH}$ component, the vortices at $(0, 0)$, $(0, 10)$, and $(10, 0)$ are circulating clockwise while the vortex at $(10, 10)$ is circulating counterclockwise. In contrast, the vortices of $\Delta_{\downarrow\downarrow}^{EH}$ have opposite chiralities, i.e.,

$$\begin{aligned}\frac{1}{2\pi} \oint ds \cdot \mathbf{F}_{\uparrow\uparrow}^{EH}(\mathbf{r})/|\mathbf{F}_{\uparrow\uparrow}^{EH}(\mathbf{r})| \\ = -\frac{1}{2\pi} \oint ds \cdot \mathbf{F}_{\downarrow\downarrow}^{EH}(\mathbf{r})/|\mathbf{F}_{\downarrow\downarrow}^{EH}(\mathbf{r})|.\end{aligned}\quad (3.35)$$

In eq. (3.35), the chiralities of $\Delta_{\uparrow\uparrow p}^{EH}(\mathbf{r})$ and $\Delta_{\downarrow\downarrow p}^{EH}(\mathbf{r})$ around a vortex are respectively defined as $\frac{1}{2\pi} \oint ds \cdot \mathbf{F}_{\uparrow\uparrow}^{EH}(\mathbf{r})/|\mathbf{F}_{\uparrow\uparrow}^{EH}(\mathbf{r})|$ and $\frac{1}{2\pi} \oint ds \cdot \mathbf{F}_{\downarrow\downarrow}^{EH}(\mathbf{r})/|\mathbf{F}_{\downarrow\downarrow}^{EH}(\mathbf{r})|$ with an integral path around the vortex.

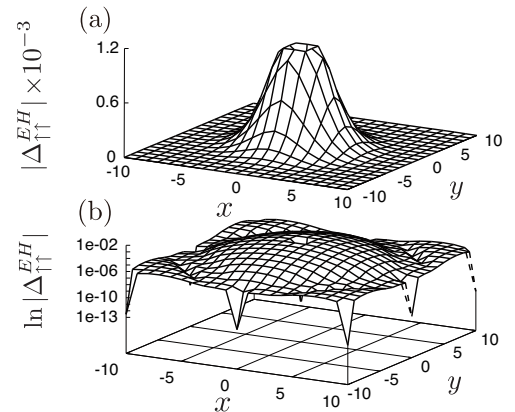


Fig. 6. Spatial dependences of (a) $|\Delta_{\uparrow\uparrow}^{EH}|$ and (b) $\ln |\Delta_{\uparrow\uparrow}^{EH}|$. Here, $|\Delta_{\uparrow\uparrow}^{EH}| = 0$ holds at the origin and is not plotted in the lower panel.

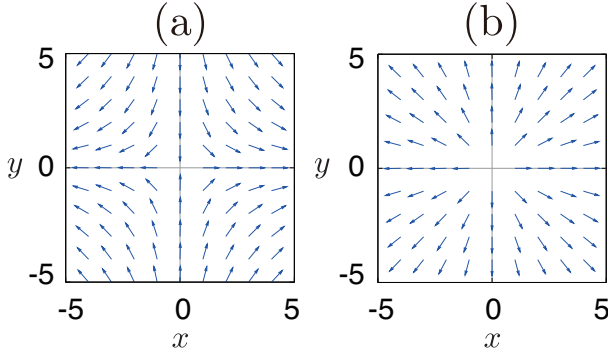


Fig. 7. (Color online) Spatial configuration of normalized vector fields, (a) $\mathbf{F}_{\uparrow\uparrow}^{EH}/|\mathbf{F}_{\uparrow\uparrow}^{EH}|$ and (b) $\mathbf{F}_{\downarrow\downarrow}^{EH}/|\mathbf{F}_{\downarrow\downarrow}^{EH}|$. The direction of the arrow represents the complex phase of $\Delta_{\uparrow\uparrow}^{EH}$ or $\Delta_{\downarrow\downarrow}^{EH}$. At singular points, where $|\mathbf{F}| = \vec{0}$ holds, the arrows are not plotted.

In the present model, the off-site p -wave components Δ_{p_x} and Δ_{p_y} exist simultaneously. They are calculated from the off-site pair potentials as

$$\Delta_{\sigma\sigma'p_i}^{\tau\tau'}(\mathbf{r}) = \frac{1}{2} \left[\Delta_{\sigma\sigma'}^{\tau\tau'}(\mathbf{r}, \mathbf{r} + \mathbf{e}_i) - \Delta_{\sigma\sigma'}^{\tau\tau'}(\mathbf{r}, \mathbf{r} - \mathbf{e}_i) \right] \quad (i = x, y). \quad (3.36)$$

Then we introduce the representation of $p_x \pm ip_y$ components as

$$\eta_{\sigma\sigma'\pm}^{\tau\tau'}(\mathbf{r}) = \frac{1}{2} (\Delta_{\sigma\sigma'p_x}^{\tau\tau'}(\mathbf{r}) \mp i\Delta_{\sigma\sigma'p_y}^{\tau\tau'}(\mathbf{r})), \quad (3.37)$$

where η_{\pm} corresponds to the $p_x \pm ip_y$ component. This representation is useful when describing the pair potential of chiral p -wave-like SCs.

Without impurities, $(\Delta_{\uparrow\uparrow p_x}^{\tau\tau'}, \Delta_{\uparrow\uparrow p_y}^{\tau\tau'})$ consists of η_- components and $(\Delta_{\downarrow\downarrow p_x}^{\tau\tau'}, \Delta_{\downarrow\downarrow p_y}^{\tau\tau'})$ consists of η_+ components. These results are consistent with the results in § 3.1. For example, since $\Delta_{\uparrow\uparrow p_x}^{EE}(x, y, z = 1) = A(1, 1) + B(1, 1)$ and $\Delta_{\uparrow\uparrow p_y}^{EE}(x, y, z = 1) = -i[A(1, 1) + B(1, 1)]$ are derived from eq. (3.26) without impurities, $\eta_{\uparrow\uparrow+}^{EE}$ vanishes and $\eta_{\uparrow\uparrow-}^{EE}$ remains.

We show the spatial structures of $\Delta_{\uparrow\uparrow}^{EE}$ and $\Delta_{\downarrow\downarrow}^{EE}$. Figure 8 shows $\eta_{\uparrow\uparrow-}^{EE}$, which is the dominant component of $\Delta_{\uparrow\uparrow}^{EE}$. This configuration is the same as that of $\eta_{\downarrow\downarrow+}^{EE}$. Figure 9 shows the absolute values of $\eta_{\uparrow\uparrow+}^{EE}$ induced by the impurity. From the spatial configuration on the logarithmic scale, we find that there are six vortices in the system. Figure 10 shows the spatial configurations of two normalized vector fields, $\mathbf{F}_{\uparrow\uparrow+}^{EE}/|\mathbf{F}_{\uparrow\uparrow+}^{EE}|$ and $\mathbf{F}_{\downarrow\downarrow-}^{EE}/|\mathbf{F}_{\downarrow\downarrow-}^{EE}|$, where

$$\mathbf{F}_{\uparrow\uparrow+}^{EE}(\mathbf{r}) = (\text{Re}[\eta_{\uparrow\uparrow+}^{EE}(\mathbf{r})], \text{Im}[\eta_{\uparrow\uparrow+}^{EE}(\mathbf{r})]), \quad (3.38)$$

and

$$\mathbf{F}_{\downarrow\downarrow-}^{EE}(\mathbf{r}) = (\text{Re}[\eta_{\downarrow\downarrow-}^{EE}(\mathbf{r})], \text{Im}[\eta_{\downarrow\downarrow-}^{EE}(\mathbf{r})]). \quad (3.39)$$

Since we fix the length of the arrows representing the vector fields, only the directions of the arrows are meaningful, which correspond to the complex phases of $\eta_{\uparrow\uparrow+}^{EE}(\mathbf{r})$ or $\eta_{\downarrow\downarrow-}^{EE}(\mathbf{r})$. At singular points, the arrows are not plotted as in Fig. 7. Since $\eta_{\uparrow\uparrow+}^{EE}$ and $\eta_{\downarrow\downarrow-}^{EE}$ have opposite chiralities,

i.e.,

$$\begin{aligned} & \frac{1}{2\pi} \oint ds \cdot \mathbf{F}_{\uparrow\uparrow+}^{EE}(\mathbf{r})/|\mathbf{F}_{\uparrow\uparrow+}^{EE}(\mathbf{r})| \\ &= -\frac{1}{2\pi} \oint ds \cdot \mathbf{F}_{\downarrow\downarrow-}^{EE}(\mathbf{r})/|\mathbf{F}_{\downarrow\downarrow-}^{EE}(\mathbf{r})|, \end{aligned} \quad (3.40)$$

the induced circular electric current of each spin component flows in opposite directions. In eq.(3.40), the chiralities of $\eta_{\uparrow\uparrow+}^{EE}$ and $\eta_{\downarrow\downarrow-}^{EE}$ around a vortex are respectively defined as $\frac{1}{2\pi} \oint ds \cdot \mathbf{F}_{\uparrow\uparrow+}^{EE}(\mathbf{r})/|\mathbf{F}_{\uparrow\uparrow+}^{EE}(\mathbf{r})|$ and $\frac{1}{2\pi} \oint ds \cdot \mathbf{F}_{\downarrow\downarrow-}^{EE}(\mathbf{r})/|\mathbf{F}_{\downarrow\downarrow-}^{EE}(\mathbf{r})|$, with an integral path around the vortex. These circulating currents represent spin currents.

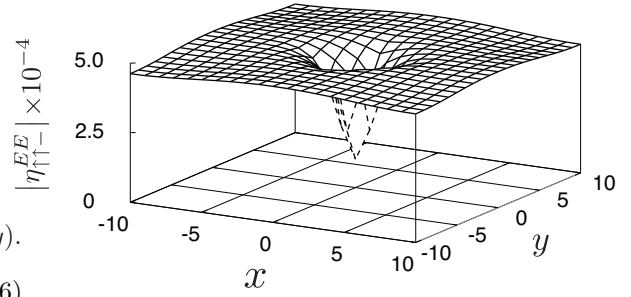


Fig. 8. Spatial dependence of $|\eta_{\uparrow\uparrow-}^{EE}|$, which is the dominant component of $\Delta_{\uparrow\uparrow}^{EE}$. This configuration is the same as $|\eta_{\downarrow\downarrow+}^{EE}|$.

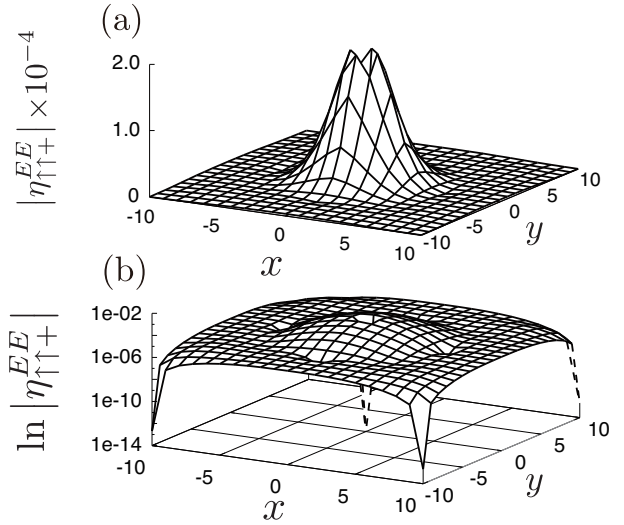


Fig. 9. Spatial dependences of (a) $|\eta_{\uparrow\uparrow+}^{EE}|$ and (b) $\ln|\eta_{\uparrow\uparrow+}^{EE}|$. These configurations are the same as $|\eta_{\downarrow\downarrow-}^{EE}|$ and $\ln|\eta_{\downarrow\downarrow-}^{EE}|$ respectively.

In this subsection, we observe the spatial structures of typical pair-potential components. For the complex phase of s -wave and p -wave components, qualitatively different spatial configurations are obtained, both of which are allowed in the original symmetry of the system. In particular, the complex phase of p -wave components around impurities should be observed as spin currents around them.

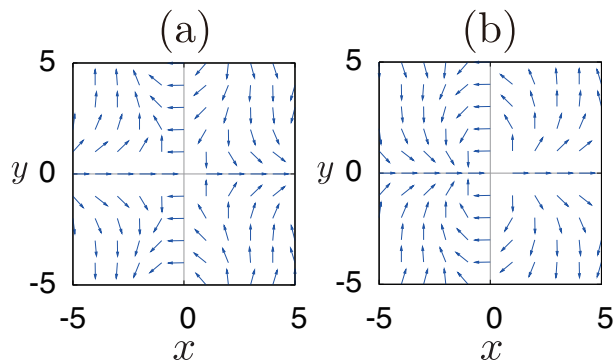


Fig. 10. (Color online) Spatial configurations of normalized vector fields, (a) $\mathbf{F}_{\uparrow\uparrow+}^{EE}/|\mathbf{F}_{\uparrow\uparrow+}^{EE}|$ and (b) $\mathbf{F}_{\downarrow\downarrow-}^{EE}/|\mathbf{F}_{\downarrow\downarrow-}^{EE}|$. The direction of the arrow represents the complex phase of $\eta_{\uparrow\uparrow+}^{EE}$ or $\eta_{\downarrow\downarrow-}^{EE}$. At singular points, where $|\mathbf{F}| = \vec{0}$ holds, the arrows are not plotted. The two opposite components have opposite chiralities.

3.5 Wave function of Bogoliubov quasi-particle

Now, we study the energy spectra and wave functions of a Bogoliubov quasiparticle composed of SSs. In the present calculation, there are eight states near the Fermi energy. Without impurities these eight states are degenerate since the system has a four-fold rotational symmetry and an inversion symmetry. By introducing an impurity potential, these states split. In Fig. 11, we show the ratio of the energy level splitting E_{imp} to the BCS energy gap E_{BCS} caused by an impurity when the system size changes. Since $E_{\text{imp}}/E_{\text{BCS}}$ is scaled to zero in the thermodynamic limit, it supports the notion that the impurity level does not split off from the gap edge. This means that the state does not develop into a mid-gap bound state.

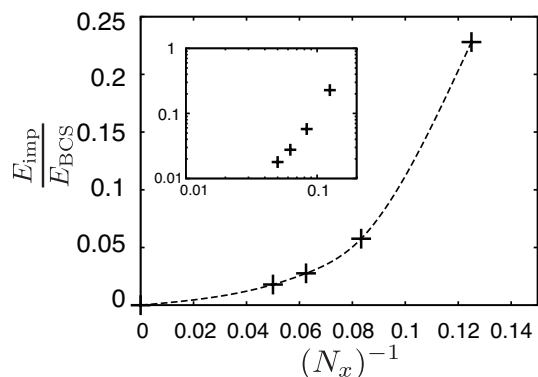


Fig. 11. Relationship between system size and ratio of energy level splitting E_{imp} to BCS energy gap E_{BCS} caused by an impurity. Inset shows a log-log plot for the same data.

In Fig. 12, the amplitude of the quasiparticle wave function that has an energy nearest to the Fermi energy is shown. This wave function is spatially extended and supports the notion that, in the thermodynamic limit, the state in Fig. 11 does not seem to reduce to a mid-gap bound state, in agreement with the absence of a bound state.

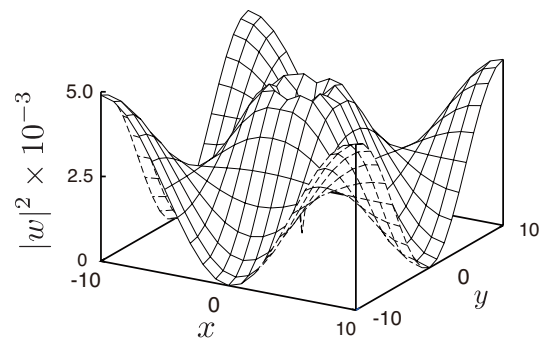


Fig. 12. Amplitude of the quasiparticle wave function for the state whose energy is the nearest to the Fermi energy.

If there were an energy level of a mid-gap or gapless state in a SC, it would not be able to penetrate the bulk due to the existence of a SC gap. Therefore, such a mid-gap state has to be bounded near the surfaces or edges of the SC. The mid-gap state is referred to as an Andreev bound state (ABS). Because the SC is a full gap SC in the 2D surface, the stability of ABSs is related to the topology of the superconducting gap; if the superconducting gap is topologically nontrivial, ABSs should be topologically protected and stable, and such a SC is called a topological SC, which is analogous in stability of SSs in TIs.

Our result supports the notion that there are no ABSs that are mid-gap states formed around the impurity. The absence of ABSs represents the notion that the superconductivity gap induced by an s -wave attractive interaction on the surfaces of TIs is topologically trivial, i.e., the present SC is not a topological SC. On the other hand, spinless chiral p -wave SCs, which have similar forms of pair potential to the present SCs, are topological SCs.¹⁴ This means that SCs on the surfaces of TIs and spinless chiral p -wave SCs are topologically different.

4. Conclusion and Discussion

In §2, we have shown that unconventional SCs induced by the s -wave attractive interaction on the surfaces of TIs are robust against TRS disorders in idealistic Dirac electron models. This is because of the cancellation of two phase factors, i.e., one from the pairing potential and the other from the scattering factor of Dirac electrons. In contrast, unconventional SCs studied in the literature, such as d -wave and chiral p -wave SCs,²³ are sensitively suppressed through scattering by a tiny concentration of impurities because of the phase factor of the pairing potential.

In §3, by numerically analyzing the Bogoliubov deGennes equation beyond the perturbative regime for impurities, we have obtained the result that SCs induced by the s -wave attractive interaction on the surfaces of TIs are stable against TRS impurities since the pair potential does not decrease linearly within a range of small concentration. This result is consistent with that discussed in §2. Moreover, we have found that the robustness is observed even when the impurity potential is strong beyond the perturbation theory. We have also found that

the reduction rate depends on the spin polarization of magnetic impurities. This is because the change in the DOS depends on the polarization.³³ This implies that the superconducting gap in the present SC is topologically trivial, i.e., the present SC is a trivial SC. Generally, the existence of ABSs and the stability of SCs are closely related, i.e., SCs that are stable against TRS impurities have ABSs around impurities. According to our results, this relation appears to be satisfied in the present SC on the surfaces of TIs.

Finally, we describe issues left for future study. In this paper, we have studied the superconductivity stabilized by an internal s -wave interaction in order to clarify fundamental impurity effects. Recently, however, superconductivity introduced by the proximity effect has also actively been studied.^{12,17} Impurity effects on the SC introduced by the proximity effect are also intriguing.

Moreover, stability against vortices is important. This is because, in realizing a Majorana bound state around a vortex,¹² the backscattering of Dirac electrons due to a magnetic field, which breaks TRS, can be destructive in terms of the stability of SSs.

Acknowledgement

Numerical calculation was partly carried out at the Supercomputer Center, Institute for Solid State Physics, The University of Tokyo. This work has been supported by Grant-in-Aid for Scientific Research from MEXT Japan under the grant numbers 22104010 and 22340090. This work has also been financially supported by MEXT HPCI Strategic Programs for Innovative Research (SPIRE) and Computational Materials Science Initiative (CMSI).

Appendix:

A.1 Symmetry operation

Here, we discuss symmetry operations that preserve spatial symmetries that the Hamiltonian in eq. (3.2) has. The symmetries of superconducting pair potentials are determined by irreducible representations of a group consisting of these symmetry operators.

First, we introduce a matrix representation of symmetry operators as follows: A symmetry operator on a Hilbert space is denoted as \mathcal{P} , while its matrix representation acting on creation (annihilation) operator-vectors \hat{P} (\hat{P}^\dagger) is defined as

$$\mathcal{P}c^\dagger\mathcal{P}^{-1} = c^\dagger\hat{P}, \quad (\text{A}\cdot 1)$$

$$\mathcal{P}c\mathcal{P}^{-1} = \hat{P}^\dagger c, \quad (\text{A}\cdot 2)$$

where \hat{P} depends on the choice of the basis.

Then the BCS mean-field Hamiltonian is transformed under a symmetry operation \mathcal{P} as

$$\mathcal{P}\mathcal{H}\mathcal{P}^{-1} = \frac{1}{2} (c^\dagger\hat{P} \ c^T\hat{P}) \begin{pmatrix} \hat{H}_0 & \hat{\Delta} \\ \hat{\Delta}^\dagger & -\hat{H}_0^T \end{pmatrix} \begin{pmatrix} \hat{P}^\dagger c \\ \hat{P}^T (c^\dagger)^T \end{pmatrix} (\text{A}\cdot 3)$$

If $\mathcal{P}\mathcal{H}\mathcal{P}^{-1} = \mathcal{H}$, i.e., $\hat{P}\hat{H}_0\hat{P}^\dagger = \hat{H}_0$ and $\hat{P}\hat{\Delta}\hat{P}^T = \hat{\Delta}$, is satisfied, the noninteracting Hamiltonian \hat{H}_0 and the order parameter matrix $\hat{\Delta}$ are both invariant under the operation \mathcal{P} .

The effective tight-binding Hamiltonian \mathcal{H}_0 of Bi_2Se_3 in §3 is invariant under the symmetry operations belonging to the point group D_{4h} . These symmetry operations are characterized by the character table given in Table A.1.

With the choice of the basis employed in this paper, we obtain matrix representation for each symmetry operation in D_{4h} , as shown in Tables A.2. and A.3. Table A.2 corresponds to the matrix acting on the spin indices and subbands indices E and H , and Table A.3 corresponds to the matrix acting on spatial coordinates. In Table A.2, we note that $\hat{\sigma}$ acts on spin indices and $\hat{\tau}$ acts on subbands indices. When we assume an s -wave attractive interaction in the effective model, we obtain pair potentials belonging to the irreducible representation A_{1g} .

Table A-1. Character table for D_{4h} point group.

D_{4h}	E	$2C_4$	C_4^2	$2C_2'$	$2C_2''$	I	S_4	σ_h	$2\sigma_v$	$2\sigma_d$	Example of basis
A_{1g}	1	1	1	1	1	1	1	1	1	1	z^2 or $x^2 + y^2$
A_{2g}	1	1	1	-1	-1	1	1	1	-1	-1	$xy(x^2 - y^2)$
B_{1g}	1	-1	1	1	-1	1	-1	1	1	-1	$x^2 - y^2$
B_{2g}	1	-1	1	-1	1	1	-1	1	-1	1	xy
E_g	2	0	-2	0	0	2	0	-2	0	0	$\{-zx, zy\}$
A_{1u}	1	1	1	1	1	-1	-1	-1	-1	-1	$xyz(x^2 - y^2)$
A_{2u}	1	1	1	-1	-1	-1	-1	-1	1	1	z
B_{1u}	1	-1	1	1	-1	-1	1	-1	-1	1	xyz
B_{2u}	1	-1	1	-1	1	-1	1	-1	1	-1	$z(x^2 - y^2)$
E_u	2	0	-2	0	0	-2	0	2	0	0	$\{x, y\}$

Table A.2. Table of transformation matrices for spin basis and subbands indices.

	$(E, H) \otimes (\uparrow, \downarrow)$
E	$I \otimes I$
$2C_4$	$\frac{1}{\sqrt{2}}I \otimes (I + i\sigma_z), \frac{1}{\sqrt{2}}I \otimes (I - i\sigma_z)$
C_4^2	$iI \otimes \sigma_z$
$2C_2'$	$iI \otimes \sigma_x, iI \otimes \sigma_y$
$2C_2''$	$\frac{i}{\sqrt{2}}I \otimes (\sigma_x + \sigma_y), \frac{i}{\sqrt{2}}I \otimes (\sigma_x - \sigma_y)$
I	$\tau_z \otimes I$
$2IC_4 = 2S_4$	$\frac{1}{\sqrt{2}}\tau_z \otimes (I + i\sigma_z), \frac{1}{\sqrt{2}}\tau_z \otimes (I - i\sigma_z)$
σ_h	$i\tau_z \otimes \sigma_z$
$2\sigma_v$	$i\tau_z \otimes \sigma_x, i\tau_z \otimes \sigma_y$
$2\sigma_d$	$\frac{i}{\sqrt{2}}\tau_z \otimes (\sigma_x + \sigma_y), \frac{i}{\sqrt{2}}\tau_z \otimes (\sigma_x - \sigma_y)$

Table A.3. Transformation for spatial coordinates.

	(x, y, z)
E	(x, y, z)
$2C_4$	$(y, -x, z), (-y, x, z)$
C_4^2	$(-x, -y, z)$
$2C_2'$	$(x, -y, -z), (-x, y, -z)$
$2C_2''$	$(y, x, -z), (-y, -x, -z)$
I	$(-x, -y, -z)$
$2IC_4 = 2S_4$	$(-y, x, -z), (y, -x, -z)$
σ_h	$(x, y, -z)$
$2\sigma_v$	$(-x, y, z), (x, -y, z)$
$2\sigma_d$	$(-y, -x, z), (y, x, z)$

A.2 Reference systems

When we analyze impurity effects on 2D superconductivities specific to those arising in the surface states of 3D TIs, we need to study those on the 2D SC in a topologically trivial reference system. As a simple reference system, here we introduce a 2D tight-binding model on a square lattice.

The Hamiltonian of the 2D tight-binding model with an s -wave attractive interaction is defined as

$$\begin{aligned} \mathcal{H} = & t \sum_{\langle i,j \rangle, \sigma} c_{i\sigma}^\dagger c_{j\sigma} - g \sum_i c_{i\uparrow}^\dagger c_{i\uparrow} c_{i\downarrow}^\dagger c_{i\downarrow} \\ & + u \sum_{i=1}^{N_i} c_{n(i)\sigma}^\dagger c_{n(i)\sigma} - \mu \sum_{i\sigma} c_{i\sigma}^\dagger c_{i\sigma}, \end{aligned} \quad (\text{A.4})$$

where t , g , u , and μ are the hopping between nearest-neighbor sites, the amplitude of the on-site attractive interaction, the impurity potential, and the chemical potential of the system, respectively. Here, $n(i)$ is the location of the i -th impurity and N_i is the number of impurities. When we consider magnetic scattering (polarized along the z -axis), we substitute

$$u_s \sum_{i=1}^{N_i} (c_{n(i)\uparrow}^\dagger c_{n(i)\uparrow} - c_{n(i)\downarrow}^\dagger c_{n(i)\downarrow}), \quad (\text{A.5})$$

for the impurity term in eq.(A.4),

$$u \sum_{i=1}^{N_i} c_{n(i)\sigma}^\dagger c_{n(i)\sigma}. \quad (\text{A.6})$$

Similarly to the effective model for Bi_2Se_3 , we introduce a mean-field decoupling with real-space order parameters Δ_i being self-consistently defined by

$$\Delta_i = g \langle c_{i\uparrow} c_{i\downarrow} \rangle. \quad (\text{A.7})$$

Note that, when $u = 0$, the order parameter Δ_i is homogeneous and obtained using

$$\begin{aligned} \Delta_i &\equiv \Delta_0, \\ \Delta_0 &= \frac{g}{S} \sum_\nu \frac{\Delta_0}{4\sqrt{E_\nu^2 + \Delta_0^2}}. \end{aligned} \quad (\text{A.8})$$

A.3 Method of compensating for change in density of states

In this subsection, we introduce a simple scheme for reducing finite-size effects in impurity effects on SC. A dominant finite size effect comes from the change in the DOS due to the introduced impurity potentials, which is assumed to be negligible in a thermodynamic limit. Then, we test the validity of the method by analyzing numerical results on the s -wave SC in the tight-binding model on the square lattice, introduced in the previous subsection, in comparison with the AG theory.

The change in the DOS is assigned as a higher-order effect and neglected in the AG theory for continuum models. However, in finite-size BdG calculations, the change in the DOS arising from the impurities quantitatively affects the order parameter, in addition to relaxation or pair-breaking processes due to impurities, while this is assumed to be negligible. Therefore, we have to compensate for this change when one wishes to estimate the genuine reduction in the order parameter purely arising from impurity relaxation processes. Here we remind the readers that the change in the DOS and the effects of the impurity relaxation processes correspond to the diagram in Figs. 1(a) and 1(b), respectively.

When we neglect such a change in the DOS, the pair potential with impurities is calculated in the perturbation regime as

$$\Delta(u, n_i) = \Delta_0 + \delta\Delta(u, n_i), \quad (\text{A.9})$$

$$\delta\Delta(u, n_i) = -\frac{\pi}{4\tau_s(u, n_i)}, \quad (\text{A.10})$$

according to the AG theory^{24,30} where u and n_i is the strength of impurity potentials and the impurity concentration, respectively. In eq.(A.9), Δ_0 is the impurity-free pair potential. In eq.(A.10), $\tau_s(u, n_i)$ is the impurity relaxation time contributing to the reduction in the order parameter. This relaxation time is determined by the strength of impurity potentials u and the impurity concentration n_i as well as the symmetries of the impurity scattering and order parameters.^{23,24}

However, in numerical solutions of the BdG equation on finite-size systems, the reduction in the order parameter is not fully given by $\delta\Delta(u, n_i)$ in eq.(A.9). We need to take into account the changes in the DOS as well. In order to subtract the reduction due to the changes in the DOS, we introduce a ‘‘relaxation-ignored’’ pair potential $\Delta_{(\text{DOS})}$, in which only the change in the DOS by

the impurities is taken into account, while the impurity relaxation times are neglected. By using the relaxation-ignored pair potential $\Delta_{(\text{DOS})}$, eq.(A-9) is replaced by

$$\Delta(u, n_i) = \Delta_{(\text{DOS})}(u, n_i) + \delta\Delta(u, n_i), \quad (\text{A}\cdot\text{11})$$

when

$$\frac{u^2 n_i N_0}{\Delta(u, n_i)} \ll 1 \quad (\text{A}\cdot\text{12})$$

holds, where N_0 is the DOS at the Fermi energy. Here, $u^2 n_i N_0$, the numerator on the left-hand side of eq.(A-12), is the same order as $\delta\Delta(u, n_i)$.

Then, we introduce an equation by which the relaxation-ignored pair potential is calculated and verify the validity of the method by analyzing s -wave SC in a tight-binding model for the square lattice. In the regime of small impurity concentration, we define the relaxation-ignored pair potential $\Delta_{(\text{DOS})}$ from the self-consistent equation

$$\Delta_{(\text{DOS})}(u, n_i) = \frac{g}{S} \sum_{\nu} \frac{\Delta_{(\text{DOS})}(u, n_i)}{4\sqrt{E_{\nu}(u, n_i)^2 + \Delta_{(\text{DOS})}(u, n_i)^2}}, \quad (\text{A}\cdot\text{13})$$

where $E_{\nu}(u, n_i)$ is the set of eigenvalues when the system has no attractive interaction but has impurities. By the estimation using eq.(A-13), we consider the change in the order parameter due to the shift in the energy spectrum. The relaxation processes are not contained in the estimate of $\Delta_{(\text{DOS})}$, because they appear as shifts in the imaginary parts of the quasiparticle energies.

The estimation of the relaxation-ignored pair potential by eq.(A-13) enables us to compensate for the change in the DOS in the BdG calculations. When we focus on the relative reduction in the pair potential purely from the impurity relaxation processes, we should concentrate on the quantity $\delta\Delta(u, n_i)/\Delta_0$, which represents the reduction. By using eq.(A-11), we introduce an equation that associates the results of the BdG calculations with the reduction of the pair potential purely due to the relaxation processes. The equation is

$$1 + \frac{\delta\Delta(u, n_i)}{\Delta_0} = \frac{\langle\langle\Delta(u, n_i)\rangle\rangle_x}_{\langle\Delta_{(\text{DOS})}(u, n_i)\rangle_{\text{imp}}}, \quad (\text{A}\cdot\text{14})$$

which is valid in the ranges of small n_i and u . Since the pair potentials obtained by the BdG calculations have spatial and impurity-configuration dependences, we take two types of averages: $\langle\cdots\rangle_x$ and $\langle\cdots\rangle_{\text{imp}}$. The average $\langle\cdots\rangle_x$ means the spatial average, i.e.,

$$\langle A \rangle_x = \frac{1}{S} \sum_{i=1}^S A_i, \quad (\text{A}\cdot\text{15})$$

where S is the system size and A_i is a quantity depending on the site i . The other average $\langle\cdots\rangle_{\text{imp}}$ represents the average over impurity configurations, i.e.,

$$\langle B \rangle_{\text{imp}} = \frac{1}{N_c} \sum_{j=1}^{N_c} B_j, \quad (\text{A}\cdot\text{16})$$

where N_c is the number of impurity configurations and

B_j is a quantity depending on the impurity configuration j . Moreover, note that we have to take Δ_{DOS} after the impurity-configuration average, since it also depends on the impurity configuration.

Then we can compare the results of the BdG with those obtained using the AG theory. By using the AG theory, the left side of eq.(A-14) is estimated as

$$1 + \frac{\delta\Delta(u, n_i)}{\Delta_0} = 1 - \frac{\pi}{4\tau_s(u, n_i)\Delta_0}. \quad (\text{A}\cdot\text{17})$$

In the cases of the TRS and magnetic scatterings, the relaxation times τ_s are obtained using

$$\frac{1}{\tau_s^{(\text{TRS})}(u, n_i)} = \mathcal{O}(n_i^2), \quad (\text{A}\cdot\text{18})$$

and

$$\frac{1}{\tau_s^{(\text{mag})}(u, n_i)} = 2\pi n_i u^2 N_0, \quad (\text{A}\cdot\text{19})$$

respectively, where N_0 is the DOS at the Fermi energy without impurities, i.e.,

$$N_0 = \frac{1}{\pi S} \sum_{\nu} \delta(\epsilon_{0\nu\uparrow}) = \frac{1}{2\pi S} \sum_{\nu} \delta(\epsilon_{0\nu}). \quad (\text{A}\cdot\text{20})$$

Here, note that, in the finite size system, the DOS is not well-defined. However, we can introduce a reasonable estimation of the DOS N_0 by reconsidering how the DOS N_0 appears in the AG theory. In the AG theory, the quantity N'_0 is replaced by the the DOS in the thermodynamic limit

$$N'_0 = \frac{1}{2\pi S} \int_0^{\tilde{\omega}} \frac{d\omega}{\tilde{\omega}} \frac{\omega}{\omega^2 + \epsilon_{0\nu}^2}, \quad (\text{A}\cdot\text{21})$$

where $\tilde{\omega}$ is the energy cutoff. We adopt $\tilde{\omega}$ as the bandwidth, i.e., $\tilde{\omega} = 8$, and estimate the DOS as $N_0 = N'_0$ even in finite-size systems.

By comparing the two estimate of $1 + \frac{\delta\Delta(u, n_i)}{\Delta_0}$ by eqs. (A-13) and (A-14), we show the validity of our method of compensating for the change in the DOS. Figures A-1 and A-2 show the scattering strength and impurity concentration dependences of the pair potential, respectively. By the analyses of both dependences, we find an agreement between the two different approaches: the AG theory and real-space BdG calculation. Therefore, we conclude that our method of compensating for the change in the DOS is valid for analyzing the impurity concentration dependence of the order parameter.

- 1) M. Z. Hasan and C. L. Kane: Rev. Mod. Phys. **82** (2010) 3045.
- 2) X.-L. Qi and S.-C. Zhang: Rev. Mod. Phys. **83** (2011) 1057.
- 3) C. L. Kane and E. J. Mele: Phys. Rev. Lett. **95** (2005) 146802.
- 4) L. Fu, C. L. Kane, and E. J. Mele: Phys. Rev. Lett. **98** (2007) 106803.
- 5) J. E. Moore and L. Balents: Phys. Rev. B **75** (2007) 121306.
- 6) R. Roy: Phys. Rev. B **79** (2009) 195322.
- 7) D. Hsieh, D. Qian, L. Wray, Y. Xia, Y. S. Hor, R. J. Cava, and M. Z. Hasan: Nature **452** (2008) 970.
- 8) D. Hsieh, Y. Xia, D. Qian, L. Wray, J. H. Dil, F. Meier, J. Osterwalder, L. Patthey, J. G. Checkelsky, N. P. Ong, A. V. Fedorov, H. Lin, A. Bansil, D. Grauer, Y. S. Hor, R. J. Cava, and M. Z. Hasan: Nature **460** (2009) 1101.
- 9) Y. Xia, D. Qian, D. Hsieh, L. Wray, A. Pal, H. Lin, A. Bansil,

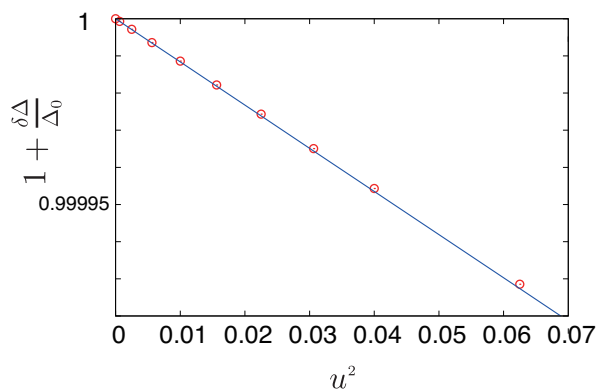


Fig. A-1. (Color online) Scattering strength dependence of pair potential for magnetic scattering. The abscissa represents the square of the strength of the impurity potential u , while the ordinate represents $1 + \delta\Delta(u, n_i)/\Delta_0$, which corresponds to a relative change in the pair potential. We take the system size as $N_x = N_y = 20$, $N_i = 1$, and $n_i = N_i/(N_x N_y) = 0.25\%$. The solid line is a theoretical estimate by the AG theory. The circle symbol corresponds to the solution of the BdG equations.

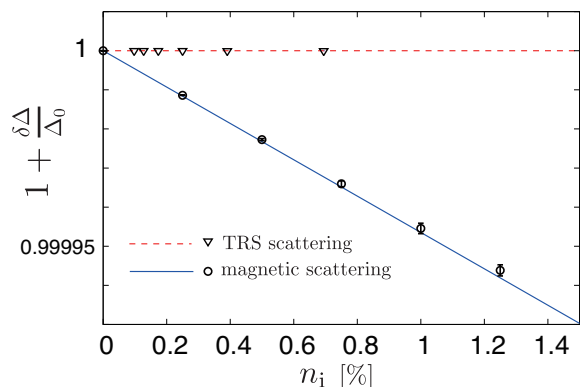


Fig. A-2. (Color online) Impurity concentration dependence of the pair potential for TRS and magnetic scatterings. The abscissa represents the impurity concentration n_i , while the ordinate represents $1 + \delta\Delta(u, n_i)/\Delta_0$. In the calculation for the TRS scattering, we fix the scattering strength to $u = 0.1$ and the number of impurities to $N_i = 1$. We alter the impurity concentration by changing the system size $N_x N_y$. In the calculation for the magnetic scattering, we fix the scattering strength to $u = 0.1$ and the system size to $N_x N_y = 400$. The solid and dashed lines are the theoretical estimates for the TRS and magnetic scatterings by the AG theory, respectively. The circle and triangle symbols correspond to the results of the TRS and magnetic scatterings by the BdG calculations, respectively.

- D. Grauer, Y. S. Hor, R. J. Cava, and M. Z. Hasan: *Nat. Phys.* **5** (2009) 398.
- 10) K. Kuroda, M. Ye, A. Kimura, S. V. Ereameev, E. E. Krasovskii, E. V. Chulkov, Y. Ueda, K. Miyamoto, T. Okuda, K. Shimada, H. Namatame, and M. Taniguchi: *Phys. Rev. Lett.* **105** (2010) 076802.
 - 11) L. Santos, T. Neupert, C. Chamon, and C. Mudry: *Phys. Rev. B* **81** (2010) 184502.
 - 12) L. Fu and C. L. Kane: *Phys. Rev. Lett.* **100** (2008) 096407.
 - 13) T. Stanescu, J. Sau, R. Lutchyn, and S. Das Sarma: *Phys. Rev. B* **81** (2010) 241310.
 - 14) N. Read and D. Green: *Phys. Rev. B* **61** (2000) 10267.
 - 15) Y. S. Hor, A. J. Williams, J. G. Checkelsky, P. Roushan, J. Seo, Q. Xu, H. W. Zandbergen, A. Yazdani, N. P. Ong, and R. J. Cava: *Phys. Rev. Lett.* **104** (2010) 057001.
 - 16) L. A. Wray, S.-Y. Xu, Y. Xia, Y. S. Hor, D. Qian, A. V. Fedorov, H. Lin, A. Bansil, R. J. Cava, and M. Z. Hasan: *Nat. Phys.* **6** (2010) 855.
 - 17) M.-X. Wang, C. Liu, J.-P. Xu, F. Yang, L. Miao, M.-Y. Yao, C. L. Gao, C. Shen, X. Ma, X. Chen, Z.-A. Xu, Y. Liu, S.-C. Zhang, D. Qian, J.-F. Jia, and Q.-K. Xue: arXiv:1112.1772
 - 18) Z. Alpichshev, J. G. Analytis, J.-H. Chu, I. R. Fisher, Y. L. Chen, Z. X. Shen, A. Fang, and A. Kapitulnik: *Phys. Rev. Lett.* **104** (2010) 016401.
 - 19) P. W. Anderson: *J. Phys. Chem. Solids* **11** (1959) 26.
 - 20) A. J. Millis, S. Sachdev, and C. M. Varma: *Phys. Rev. B* **37** (1988) 4975.
 - 21) R. J. Radtke, K. Levin, H.-B. Schüttler, and M. R. Norman: *Phys. Rev. B* **48** (1993) 653.
 - 22) R. Balian and N. R. Werthamer: *Phys. Rev.* **131** (1963) 1553.
 - 23) A. V. Balatsky, L. Vekhter, and J.-X. Zhu: *Rev. Mod. Phys.* **78** (2006) 373.
 - 24) A. A. Abrikosov and L. P. Gor'kov: *Sov. Phys. JETP* **12** (1961) 1243.
 - 25) Y. Ito, Y. Yamaji, and M. Imada: *J. Phys. Soc. Jpn.* **80** (2011) 063704.
 - 26) H. J. Zhang, C.-X. Liu, X.-L. Qi, X. Dai, Z. Fang, and S.-C. Zhang: *Nat. Phys.* **5** (2009) 438.
 - 27) C.-X. Liu, X.-L. Qi, H. J. Zhang, X. Dai, Z. Fang, and S.-C. Zhang: *Phys. Rev. B* **82** (2010) 045122.
 - 28) T. Ando, T. Nakanishi, and R. Saito: *J. Phys. Soc. Jpn.* **67** (1998) 2857.
 - 29) X.-L. Qi, T. L. Hughes, S. Raghu, and S.-C. Zhang: *Phys. Rev. Lett.* **102** (2009) 187001.
 - 30) V. Ambegaokar and A. Griffin: *Phys. Rev.* **137** (1965) A1151.
 - 31) V. L. Berezinskii: *Sov. Phys. JETP* **34** (1972) 610.
 - 32) J. M. Kosterlitz and D. J. Thouless: *J. Phys. C* **6** (1973) 1181.
 - 33) R. R. Biswas and A. V. Balatsky: *Phys. Rev. B* **81** (2010) 233405.